DAVID W. TAYLOR NAVAL SHIP
RESEARCH AND DEVELOPMENT CENTER
Bethesda, Md. 20084

A COMPARISON BETWEEN A SIMPLE DRAG FORMULA AND EXPERIMENTAL DRAG DATA FOR BODIES OF REVOLUTION

by
Nadine M. White

SHIP PERFORMANCE DEPARTMENT
RESEARCH AND DEVELOPMENT REPORT

January 1977

Report 77-0028

MAJOR DTNSRDC ORGANIZATIONAL COMPONENTS

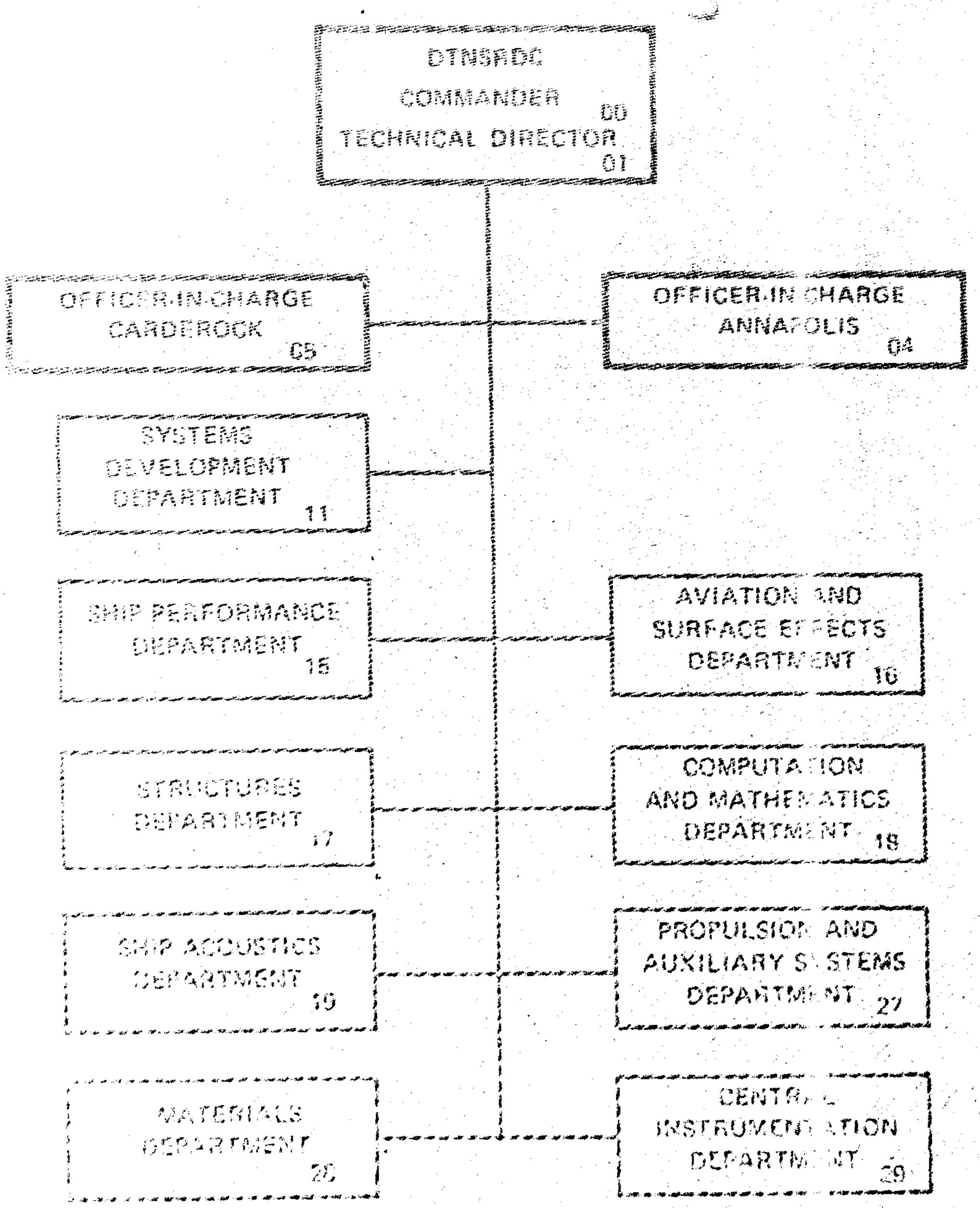

UNCLASSIFIED

SECURITY CLASSIFICATION OF THIS PAGE (When Data Entered)

REPORT DOCUMENTATION PAGE

READ INSTRUCTIONS BEFORE COMPLETING FORM

1. REPORT NUMBER: DTNSRDC [illegible]-77-0028	2. GOVT ACCESSION NO.
3. RECIPIENT'S CATALOG NUMBER	
4. TITLE (and Subtitle): A Comparison Between a Simple Drag Formula and Experimental Drag Data for Bodies of Revolution	5. TYPE OF REPORT & PERIOD COVERED: Final
6. PERFORMING ORG. REPORT NUMBER	
7. AUTHOR(s): Nadine M. White	8. CONTRACT OR GRANT NUMBER(s)
9. PERFORMING ORGANIZATION NAME AND ADDRESS: David W. Taylor Naval Ship R&D Center, Bethesda, Maryland 20084	10. PROGRAM ELEMENT, PROJECT, TASK AREA & WORK UNIT NUMBERS: Task Area [illegible]6007, Task 08101 SGL PE 63564N, Work Unit 1552-135
11. CONTROLLING OFFICE NAME AND ADDRESS: Naval Sea Systems Command, Washington, DC 20362	12. REPORT DATE: Jan[illegible]77
	13. NUMBER OF PAGES: 66
14. MONITORING AGENCY NAME & ADDRESS (if different from Controlling Office)	15. SECURITY CLASS. (of this report): UNCLASSIFIED
	15a. DECLASSIFICATION/DOWNGRADING SCHEDULE

16. DISTRIBUTION STATEMENT (of this Report)

APPROVED FOR PUBLIC RELEASE: DISTRIBUTION UNLIMITED

17. DISTRIBUTION STATEMENT (of the abstract entered in Block 20, if different from Report)

18. SUPPLEMENTARY NOTES

19. KEY WORDS (Continue on reverse side if necessary and identify by block number)

Bodies of Revolution
Drag Computation
Order of Merit Prediction
Pressure Distributions

20. ABSTRACT (Continue on reverse side if necessary and identify by block number)

A simplified drag formula used by Hess and James to predict the drag of a small number of axisymmetric forms is systematically applied to seven series of model forms comprising nearly fifty bodies. Calculations of form (or residual) drag are compared to available experimental data in order to determine the usefulness of the method for predictive purposes. The formula is shown to exhibit very little sensitivity to changes in most body parameters such as the length-of-stern to diameter ratio, nose and tail radii parameters,

DD FORM 1 JAN 73 1473 EDITION OF 1 NOV 65 IS OBSOLETE
S/N 0102-014-6601

UNCLASSIFIED

SECURITY CLASSIFICATION OF THIS PAGE (When Data Entered)

and the prismatic coefficient. For some parameters, such as length to diameter ratio, the length of bow section to diameter ratio, however, the formula is sometimes able to discriminate bodies having high values of form drag. It is concluded that the simple drag formula may not be reliably used for estimating the relative form drags of bodies of revolution.

TABLE OF CONTENTS

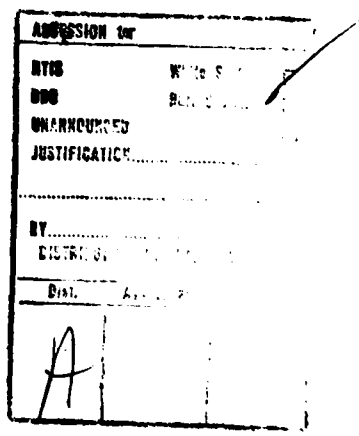

LIST OF FIGURES

LIST OF TABLES

ABSTRACT

A simplified drag formula used by Hess and James to predict the drag of a small number of axisymmetric forms is systematically applied to seven series of model forms comprising nearly fifty bodies. Calculations of form (or residual) drag are compared to available experimental data in order to determine the usefulness of the method for predictive purposes. The formula is shown to exhibit very little sensitivity to changes in most body parameters such as the length-of-stern to diameter ratio, nose and tail radii parameters, and the prismatic coefficient. For some parameters, such as length to diameter ratio, and length of bow section to diameter ratio, however, the formula is sometimes able to discriminate bodies having high values of form drag. It is concluded that the simple drag formula may not be reliably used for estimating the relative form drags of bodies of revolution.

ADMINISTRATIVE INFORMATION

This work was authorized and funded by the Naval Sea Systems Command, Task Area SS166007, Task 08101, Work Unit 1552-135.

INTRODUCTION

In a recent report[1] and paper,[2] Hess and James compare the predictions of a simple drag formula with experimental data for eight Series 58 bodies of revolution.[3] The small number of bodies used by Hess and James to justify their use of this simple formula is deemed insufficient to establish the method's validity. The present investigation attempts to remedy this by making systematic tests of the formula on many more axisymmetric bodies for which drag data are available. This study attempts to determine whether or

[1] Hess, John L. and R.N. James, "On the Problem of Shaping an Axisymmetric Body to Obtain Low Drag at Large Reynolds Numbers," McDonnell Douglas Corporation Report MDC-J6791 (Jan 1975).

[2] Hess, John L., "On the Problem of Shaping an Axisymmetric Body to Obtain Low Drag at Large Reynolds Numbers," Journal of Ship Research, Vol. 20, No. 1 (May 1976).

[3] Gertler, Morton, "Resistance Experiments on a Systematic Series of Streamlined Bodies of Revolution - For Application to the Design of High-Speed Submarines," David Taylor Model Basin Report C-297 (Apr 1950), declassified 27 Jan 1967.

not the simple formula can predict the same order of "drag" merit as that measured experimentally for a series of bodies of revolution. Even if the drag coefficients are not in excellent numerical agreement, the formula might be useful as a relative indicator of drag characteristics.

THE SIMPLE DRAG FORMULA

The drag of a body is usually calculated in one of two ways: (1) by integration of local surface-pressure and skin-friction forces acting on the body surface, or (2) by determination of the velocity profile and momentum defect in the wake far downstream of the body where the pressure is equal to the ambient pressure. Young[4] and Granville[5] provide outlines of the derivation of the momentum integral for the latter method which gives the total drag, D, of a body of revolution as

$$D = 2\pi\rho \int_0^\infty u\,(U_\infty - u)\,r\,dr \qquad [1]$$

where U_∞ = velocity of incoming flow

u = velocity of the fluid in the wake

r = radial distance from the x axis

ρ = fluid density

The general body orientation and parameter notation can be found in Figure 1.

If we define the momentum area Ω as

$$\Omega = \int_0^\delta \frac{u}{U_\infty}\left(1 - \frac{u}{U_\infty}\right) r\,dr \qquad [2]$$

where δ is the half-thickness of the wake, then, for the wake far downstream $\Omega = \Omega_\infty$, with $\delta \to \infty$ and

[4] Young, A.D., "The Calculation of the Total and Skin Friction Drag of Bodies of Revolution at Zero Incidence," Aeronautical Research Committee R&M Report 1874 (Apr 1939).

[5] Granville, P.S., "The Calculation of the Viscous Drag of Bodies of Revolution," DTMB Report 849 (Jul 1953).

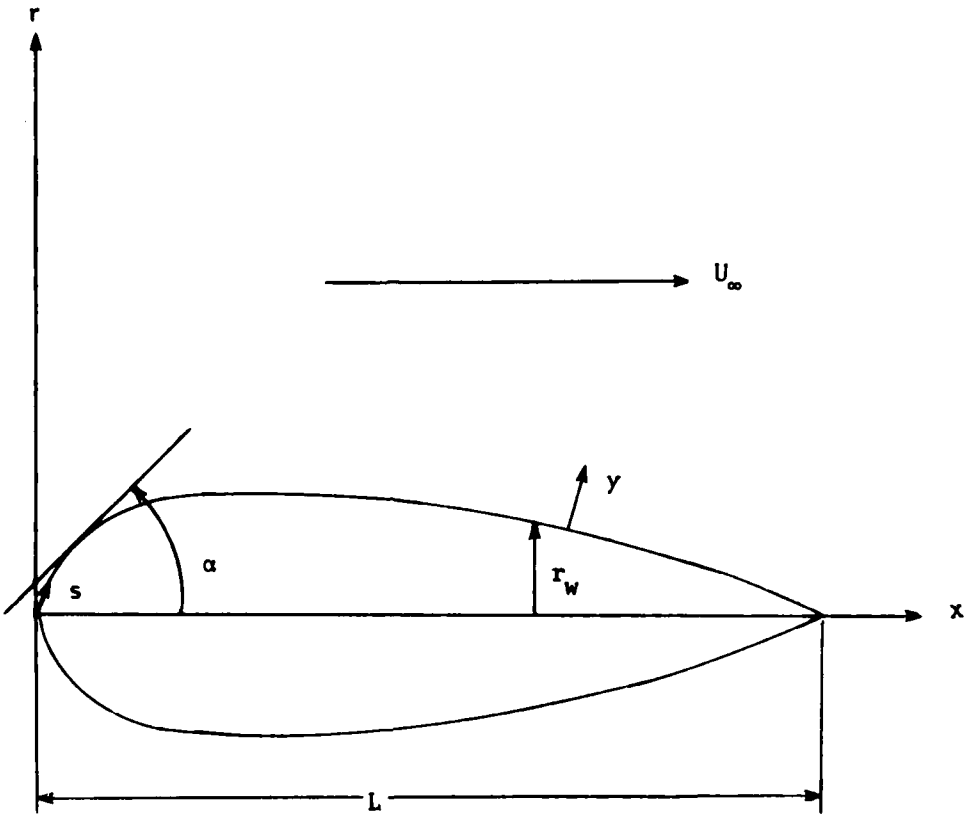

Figure 1 - Body Orientation

$$D = 2\pi\rho\, U_\infty^{\,2}\, \Omega_\infty \qquad [3]$$

Hence, for a drag coefficient, C_D, based on wetted surface area A

$$C_D = \frac{D}{1/2\rho U_\infty^{\,2} A} = \frac{4\pi\Omega_\infty}{A} \qquad [4]$$

Young[4] indicated that the wake downstream of a body is actually a continuation of the boundary layer on the body tail. Thus, boundary layer theory may be used to determine the momentum area, Ω, at the end of the tail. Then, it is necessary to relate Ω at the body tail to Ω_∞ far downstream.

For turbulent flow, the equations of motion are given by the Reynolds equations (the averaged Navier-Stokes equations). For axisymmetric flow past a body of revolution having sufficiently small longitudinal curvature, the equations of motion from Reference 5 are

$$\text{x: } u\frac{\partial u}{\partial x} + v\frac{\partial u}{\partial y} + \frac{1}{\rho}\frac{\partial P}{\partial x} = \frac{\nu}{r}\frac{\partial}{\partial y}\left[r\left(\frac{\partial u}{\partial y} - \frac{\partial v}{\partial x}\right)\right] + \frac{1}{\rho r}\frac{\partial}{\partial x}\left[p(-\rho\overline{(u')^2})\right] + \frac{1}{\rho r}\frac{\partial}{\partial y}\left[r(-\rho\overline{u'v'})\right] + \frac{\overline{(w')^2}}{r}\frac{\partial r}{\partial y} \qquad [5]$$

$$\text{y: } u\frac{\partial v}{\partial x} + v\frac{\partial v}{\partial y} + \frac{1}{\rho}\frac{\partial P}{\partial y} = \frac{\nu}{r}\frac{\partial}{\partial x}\left[r\left(\frac{\partial v}{\partial x} - \frac{\partial u}{\partial y}\right)\right] + \frac{1}{\rho r}\frac{\partial}{\partial y}\left[r(-\rho\overline{(v')^2})\right] + \frac{1}{\rho r}\frac{\partial}{\partial x}\left[r(-\rho\overline{u'v'})\right] + \frac{\overline{(w')^2}}{r}\frac{\partial r}{\partial y} \qquad [6]$$

$$\phi\text{: } o = \frac{\partial}{\partial x}\left[r(-\rho\overline{u'w'})\right] + \frac{\partial}{\partial y}\left[r(-\rho\overline{v'w'})\right] + (-\rho\overline{u'w'})\frac{\partial r}{\partial x} (-\rho\overline{v'w'})\frac{\partial r}{\partial y} \qquad [7]$$

where x, y, ϕ are body of revolution coordinates (see Figure 1) with average velocity components u, v, and w = 0 and turbulent velocity components u', v' and w'.

The continuity equation is given by

$$\frac{\partial(ru)}{\partial x} + \frac{\partial(rv)}{\partial y} = 0 \qquad [8]$$

Now, using Prandtl's assumption that the boundary layer is thin, and assuming that the Reynolds number is of order $1/\delta^2$, $\partial/\partial x << \partial/\partial y$, $\frac{\partial}{\partial y} \sim 1/\delta$ and $\frac{\partial^2}{\partial y^2} \sim \frac{1}{\delta^2}$ such that v' is of order δ and u, u', $\partial/\partial x$ and r are of order 1, equations [5-7] reduce to

$$u\frac{\partial u}{\partial x} + v\frac{\partial u}{\partial y} = -\frac{1}{\rho}\frac{\partial P}{\partial x} - \frac{1}{\rho r}\frac{\partial}{\partial x}\left[r\rho\overline{u'v'}\right] + \frac{1}{\rho r}\frac{\partial}{\partial y}\left[r\left(\mu\frac{\partial u}{\partial y} - \rho\overline{u'v'}\right)\right] \qquad [9]$$

with $\frac{\partial P}{\partial y} = 0$

For additional information on the process of reduction see Reference 6. Integration of equation [9] across the boundary layer from y = 0 to y = δ, with use of the continuity equation [8] and the definition of equation [2], gives the momentum equation for axisymmetric turbulent boundary layers on bodies of revolution:

$$\int_0^{\delta}\left(1-\frac{u}{U_\infty}\right)r\,dy \qquad [10]$$

where $h = \dfrac{\int_0^{\delta}\left(1-\frac{u}{U_\infty}\right)r\,dy}{\int_0^{\delta}\frac{u}{U_\infty}\left(1-\frac{u}{U_\infty}\right)r\,dy}$, the axisymmetric shape factor

$\tau = \mu\dfrac{\partial u}{\partial y} - \rho\overline{u'v'}$, shear stress

$\sigma = \rho\,(\overline{u'})^2$

r_w, τ_w = values of r and τ at the wall,

U = velocity at the edge of the wake

---

[6] Schlichting, H., Boundary Layer Theory, McGraw Hill, New York, 1968.

If it is assumed that $(u')^2/u^2 << 1$, then for wake flow having no wall shear this reduces nicely to

$$\frac{\partial \Omega}{\partial x} + (h + 2)\frac{\Omega}{U_\infty}\frac{\partial U}{\partial x} = 0 \qquad [11]$$

The conditions at the end of the body (denoted by subscript "e") can be related to conditions downstream in the wake by integrating [11] by parts. This yields

$$\Omega_\infty = \Omega_e \left(\frac{U_e}{U_\infty}\right)^{(h_e+2)} \exp\left[\int_1^{h_e} \ln\frac{U_\infty}{u}\, dh\right] \qquad [12]$$

Several experimental curve fittings for this equation have been made, among them fits by Young[4] and Granville.[5] Granville suggest using

$$\frac{\ln\left(\frac{U_\infty}{U}\right)}{\ln\left(\frac{U_\infty}{U_e}\right)} = \left(\frac{h-1}{h_e-1}\right)^q \qquad [13]$$

where q is determined experimentally. If this is substituted into [12], there results

$$\Omega_\infty = \Omega_e \left(\frac{U_e}{U_\infty}\right)^{\frac{(h_e+2)q+3}{1+q}} \qquad [14]$$

which when substituted into [4] yields

$$C_D = \frac{4\pi}{A}\Omega_e \left(\frac{U_e}{U_\infty}\right)^{\frac{(h_e+2)q+3}{1+q}} \qquad [15]$$

To obtain Ω_e it is necessary to return to equation [10]. Under the same assumptions made in deriving equation [11], Granville[7] develops a relation for bodies of revolution having thin boundary layers,

[7] Granville, P.S., "Partial Form Factors from Equivalent Bodies of Revolution for the Froude Method of Predicting Ship Resistance," SNAME First Ship Technology and Research Symposium, Washington, D.C. (Aug 1975).

$$\frac{d\Omega}{dS} + (h+2)\frac{\Omega}{U_\infty}\frac{dU}{dS} = \frac{r_w \tau'_w}{\rho U_\infty^2} \qquad [16]$$

where the derivative is in terms of ds instead of dx ($dx = \sec\alpha\, ds$). Here

s = distance along the body meridian

r_w = the radial distance of the body

τ'_w = wall shear stress = $\tau_w \sec\alpha$

U = the velocity at the edge of the boundary layer.

Granville[7] extends the formulation to thick axisymmetric boundary layers writing

$$\frac{\tau'_w}{\rho U_\infty^2} = \frac{k}{\left(\frac{U_\infty \Omega}{\nu r_w}\right)^m}$$

where k and m are constants, and ν is the kinematic viscosity of the fluid. Then assuming that h = constant = h_e the momentum equation [16] may be integrated to give:

$$\left(\frac{U_e}{U_\infty}\right)^{(1+m)(h+2)} \left(\frac{\Omega_e}{L^2}\right)^{(1+m)} = \frac{(1+m)k}{(Rn_L)^m} \int_0^1 \left(\frac{r_w}{L}\right)^{(1+m)} \left(\frac{U}{U_\infty}\right)^{[(1+m)(h+2)-m]} \sec\alpha\, d\left(\frac{x}{L}\right) \qquad [17]$$

where

L = body length

Rn_L = Reynolds number based on Length = $\frac{u_\infty L}{\nu}$

α = angle between the body axis and a tangent to the meridian at given x

Substitution of the value of Ω_e determined from [17] into [15] gives the drag formula

$$C_D = \frac{4\pi L^2}{A}\left(\frac{U_e}{U_\infty}\right)^{\frac{1-h}{1+q}}\left\{\frac{(1+m)k}{(Rn_L)^m}\int_0^1\left(\frac{r_w}{L}\right)^{(1+m)}\left(\frac{U}{U_\infty}\right)^{[(1+m)(h+2)-m]}\sec\alpha\, d\left(\frac{x}{L}\right)\right\}^{\frac{1}{1+m}} \qquad [18]$$

For a flat plate $U = U_\infty$, $\sec\alpha = 1$, and $r_w = A/2\pi L$, so that the drag coefficient C_D reduces to a frictional drag coefficient, C_f, given by

$$C_f = 2\left[\frac{(1+m)k}{(Rn_L)^m}\right]^{\frac{1}{1+m}}$$

which, if substituted into equation [18] gives

$$\frac{C_D}{C_f} = \frac{2\pi L^2}{A}\left(\frac{U_e}{U_\infty}\right)^{\left(\frac{1-h}{1+q}\right)}\left[\int_0^1\left(\frac{r_w}{L}\right)^{(1+m)}\left(\frac{U}{U_\infty}\right)^{[(1+m)(h+2)-m]}\sec\alpha\, d\left(\frac{x}{L}\right)\right]^{\frac{1}{1+m}} \qquad [19]$$

where C_f is the frictional drag coefficient of a flat plate having the same length and Reynolds number as the body of revolution being considered. Now, equation [19] is a general form of the simple drag formula derived in different ways by Granville[7] and Hess.[2] Values of m, q, and h employed by the two authors are

Granville: $m = 0.1686$, $q = 7$, $h = 1.4$

Hess: $m = 1/6$, $q = 1$, $h = 1$

It should be noted that Hess's numbers were derived from work by Truckenbrodt[8] and Falkner.[9] For this report, the values used were those chosen by Hess for his work. Thus, formula [19] reduces to

$$\frac{C_D}{C_f} = \frac{2\pi L^2}{A}\left[\int_0^1\left(\frac{r_w}{L}\right)^{7/6}\left(\frac{U}{U_\infty}\right)^{10/3}\sec\alpha\, d\left(\frac{x}{L}\right)\right]^{6/7} \qquad [20]$$

[8] Truckenbrodt, E., "A Method of Quadrature for Calculation of the Laminar and Turbulent Boundary Layer in Case of Plane and Rotationally Symmetrical Flow," NACA TM Report 1379 (May 1955).

[9] Falkner, V.N., Aircraft Engineering, 15 (1943), p. 65.

OUTLINE OF COMPUTATIONS

Point-generating computer programs were developed to give an accurate physical representation of each body surface for computer use. The creation of these point distributions usually involved using the original model drawings or offsets to obtain a fairly accurate curve. A least-squares polynomial fit was then passed through the data points to insure smooth rates of change in r. Two series of bodies were an exception to this; they were generated analytically by using the appropriate functions from which they were developed. The points generated were fed into an existing Douglas-Neumann axisymmetric-body program, DA50,[10] to compute the distributions of potential-flow velocity $U/U_\infty \cos \alpha$, and pressure coefficient, C_p.

With the output of the axisymmetric program, calculations of the integrand $(U/U_\infty)^{10/3} (r/L)^{7/6} \sec \alpha$, appearing in formula [20], were made and graphed against x/L. Typical distributions of the integrand are shown in Figure 2. The solid curve illustrates the integrand for a model with parallel middle body and the broken line indicates the integrand for a typical model having no parallel middle body. Using data points spaced every 0.5 percent for the first 20 percent of the body and every 1 percent thereafter, a fine grid integration was performed to compute C_D/C_f. Spacings this fine were required to achieve accurate computer results.

Since most publications report the residuary-drag coefficient C_R which is defined by $C_R = C_D - C_f$, instead of C_D, C_R/C_f was also calculated. Comparisons between computational results and experimental data were made on the basis of C_R/C_f and C_R.

No attempt is made in this report to evaluate the accuracy of the available experimental data, some of which may have been subject to error. Comparisons are made only on relative order of merit as found by the various experimenters and as computed by the simplified formula.

RESULTS

Seven series of bodies were used to test the simple drag formula: (1) the Series 58 bodies investigated by Gertler,[3] (2) Series 5242 sterns

[10] Hess, J.L. and A.M.O. Smith, "Calculation of Potential Flow About Arbitrary Bodies," in "Progress in Aeronautical Sciences," Pergamon Press, Oxford and New York, Vol. 8 (1966), pp. 1-138.

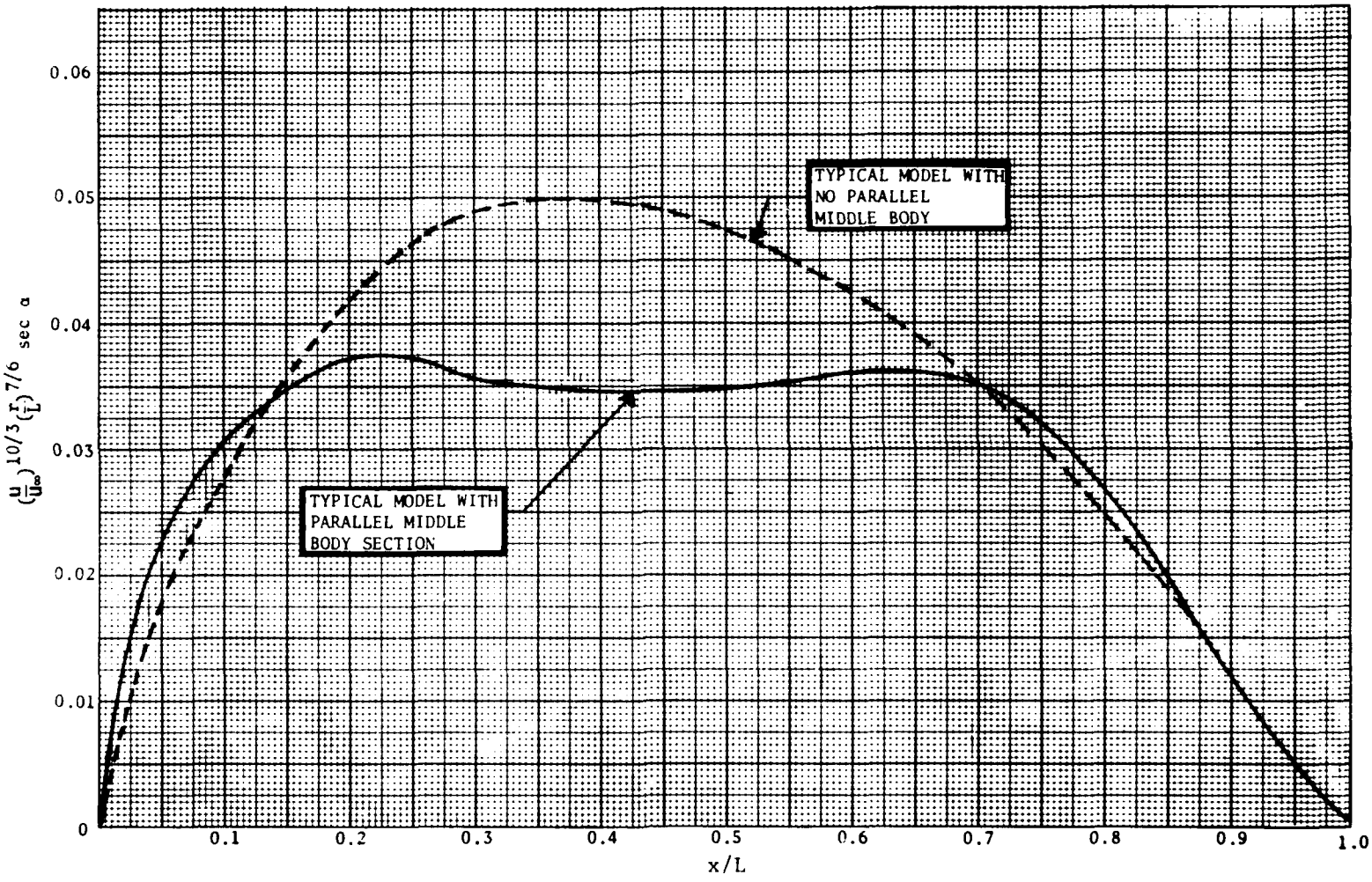

Figure 2 - Typical Curves for $\left(\frac{U}{U_\infty}\right)^{10/3}$ $(r/L)^{7/6}$ Sec α versus x/L

(unpublished), (3) six bodies with inflected sinusoidal sterns investigated by Kempf (herein after referred to as "Kempf bodies"),[11,12] (4) a series of bodies based on the best Series 58 model with various amounts of parallel middle body as reported by Larsen,[13] (5) Series 4620 forebodies investigated by McCarthy, Power, and Huang,[14] (6) polynomial representations of five miscellaneous models and finally, (7) Series 4935 afterbodies (unpublished).

Series 58

The first series of bodies was Series 58, originally developed by Gertler[3] and extensively studied by Landweber and Macagno.[15] This series is a family of bodies of revolution with sectional-area curves represented by sixth-degree polynomials. The coefficients of the equations depend on six geometric quantities: body length, L, maximum diameter, d, radii of curvature at the nose and tail, R_o and R_1, body volume, V, and axial position of body diameter, x_m. From these six parameters, several nondimensional quantities were formed and used by Landweber and Macagno to study variations in body shape. The nondimensional quantities used were length-to-diameter ratio, $\lambda = L/d$, position of maximum section, $m = x_m/L$, nondimensional nose and tail radii, $r_o = R_o L/d^2$ and $r_1 = R_2 L/d^2$, and the prismatic coefficient, $C_p = 4V/\pi L d^2$.

Nondimensional potential flow velocities on the surfaces of the Series 58 bodies were published by Landweber and Macagno[15] and were used here in computing the values of C_R/C_f by the simple formula, equation [20]. Sketches of the bodies can be found in reference 15 as can the computed pressure distributions.

---

[11] Kempf, George, "Resistance and Wake of Some Bodies of Revolution," from "New Developments in Ship Research," Jahrbuch Schiffbautechnischen Gesellschaft (1927), pp. 177-178.

[12] Kempf, George, "Turbulent Separation on Full Ship Forms," Schiff und Hafen, Vol. 6, No. 7, Hamburg (1954).

[13] Larsen, C.A., "Additional Tests of Series 58 Forms, Part 1, Resistance Tests of a Parallel Middle Body Series," David Taylor Model Basin Report C-738 (Nov 1955), declassified on 2 Sep 1975.

[14] McCarthy, J.H., J. Power, and T.T. Huang, "The Roles of Transition, Laminar Separation and Turbulence Stimulation in the Analysis of Axisymmetric Body Drag," to be published in the Proceedings of the Eleventh ONR Symposium on Naval Hydrodynamics, sponsored by the Office of Naval Research, London, (Mar 1976).

[15] Landweber, L. and Matilde Macagno, "Potential Flow about Series 58 Bodies in General Translational and Rotational Motion," Naval Ship Research and Development Center Report 2505 (Jun 1967).

TABLE 1

C_R Comparisons for Series 58

Body No.	Experimental $C_R \times 10^3$	Calculated C_R/C_f Simple Formula	Calculated $C_R^* \times 10^3$	Experimental Order of merit	Computed order of merit simple formula
4154	0.58	0.184	0.48	24	24
4155	0.36	0.141	0.37	21	23
4156	0.22	0.115	0.30	18	20
4157	0.13	0.089	0.23	6	16
4158	0.09	0.068	0.18	3	3
4159	0.075	0.043	0.11	2	1
4160	0.12	0.078	0.21	5	5
4161	0.15	0.080	0.21	12	6
4162	0.17	0.084	0.22	15	8
4163	0.19	0.084	0.22	17	9
4164	0.37	0.092	0.24	22	17
4165	0.07	0.088	0.23	1	14
4166	0.28	0.092	0.24	19	18
4167	0.16	0.094	0.25	13	19
4168	0.14	0.085	0.22	10	11
4169	0.14	0.088	0.23	11	15
4170	0.18	0.077	0.20	16	4
4171	0.13	0.063	0.17	7	2
4172	0.13	0.082	0.22	8	7
4173	0.13	0.085	0.22	9	12
4174	0.10	0.084	0.22	4	10
4175	0.32	0.137	0.36	20	22
4176	0.41	0.133	0.35	23	21
4177	0.16	0.087	0.23	14	13

Based on $Rn_L = 20 \times 10^6$

$C_f = 2.628 \times 10^{-3}$ (Schoenherr[16])

For easy reference, the computed pressure distributions are included here in Appendix A, Figures 1a through 7A.

Table 1 shows the results for the Series 58 bodies ordered by model number. The order of merit shown is measured relative to the model having the smallest experimental value of C_R. It is apparent that for the overall series, the computed orders of merit are quite different from the experimentally determined orders of merit. The best body according to Gertler's experiments was 4165. This is No. 14 in order of merit according to the simple formula. The only agreement is in the relative placement of bodies 4158, 4160, and 4154. The calculated values of C_R shown in Table 1 were computed from C_R/C_f using the constant value of C_f appropriate to a Reynolds number of 20×10^6; this value of C_f was also used by Hess[2] for his comparisons.

As mentioned above, several nondimensional parameters were formed from the geometric properties of the Series 58 models. These nondimensional quantities were varied systematically to create several subseries within the overall model range covered. Tables 2, 3, 4, 5, and 6 list the bodies involved in these series and compare the experimental results with the drag predictions of the simple formula. Figure 3 provides a graphical comparison between the experimental and calculated values of C_R. Points are labeled in terms of the major parameter varied, and not by body number.

TABLE 2

Series 58 Body Variations in L/D

($m = 0.40$, $C_p = 0.65$, $r_o = 0.5$, $r_1 = 0.1$)

Model Number	L/D	Experimental $C_R \times 10^3$ Gertler	Computer C_R/C_f Simple Formula	Computed[3] $C_R^* \times 10^3$ Simple Formula
4154	4.0	0.58	0.184	0.48
4155	5.0	0.36	0.141	0.37
4156	6.0	0.22	0.115	0.30
4157	7.0	0.13	0.089	0.23
4158	8.0	0.09	0.068	0.18
4159	10.8	0.075	0.043	0.11

*Based on $Rn_L = 20 \times 10^6$ (16)

TABLE 3

Series 58 Body Variation in m, Maximum Thickness Position

($L/D = 7.0$, $C_p = 0.65$, $r_o = 0.5$, $r_1 = 0.1$)

Model Number	m	Experimental $C_R \times 10^3$ Gertler	Computed C_R/C_f Simple Formula	Computed C_R* Simple Formula
4160	0.36	0.12	0.078	0.21
4161	0.44	0.15	0.080	0.21
4162	0.48	0.17	0.084	0.22
4163	0.52	0.19	0.084	0.22

TABLE 4

Series 58 Body Variations in C_p, The Prismatic Coefficient

($L/D = 7.0$, $m = 0.4$, $r_o = 0.5$, $r_1 = 0.1$)

Model Number	C_p	Experimental $C_R \times 10^3$ Gertler	Computed C_R/C_f Simple Formula	Computed C_R* Simple Formula
4164	0.55	0.37	0.092	0.24
4165	0.60	0.07	0.088	0.23
4166	0.70	0.28	0.092	0.24

*Based on $Rn_L = 20 \times 10^6$

$C_f = 2.638 \times 10^{-3}$ (16)

TABLE 5

Series 58 Body Variations in r_o, Nondimensional Nose Radius

($L/D = 7.0$, $C_p = 0.65$, $m = 0.4$, $r_1 = 0.1$)

Model Number	r_o	Experimental $C_R \times 10^3$ Gertler	Computed C_R/C_f Simple Formula	Computed C_R* Simple Formula
4167	0.00	0.16	0.094	0.25
4168	0.30	0.14	0.085	0.22
4169	0.70	0.14	0.088	0.23
4170	1.00	0.18	0.077	0.20

TABLE 6

Series 58 Body Variations in r_1, Nondimensional Tail Radius

($L/D = 7.0$, $C_p = 0.65$, $m = 0.4$, $r_o = 0.5$)

Model Number	r_1	Experimental $C_R \times 10^3$ Gertler	Computed C_R/C_f Simple Formula	Computed C_R* Simple Formula
4171	0.00	0.13	0.063	0.17
4172	0.05	0.13	0.082	0.22
4173	0.15	0.13	0.085	0.22
4174	0.20	0.10	0.084	0.22

*Based on $Rn_L = 20 \times 10^6$ (16)
$C_f = 2.628 \times 10^{-3}$

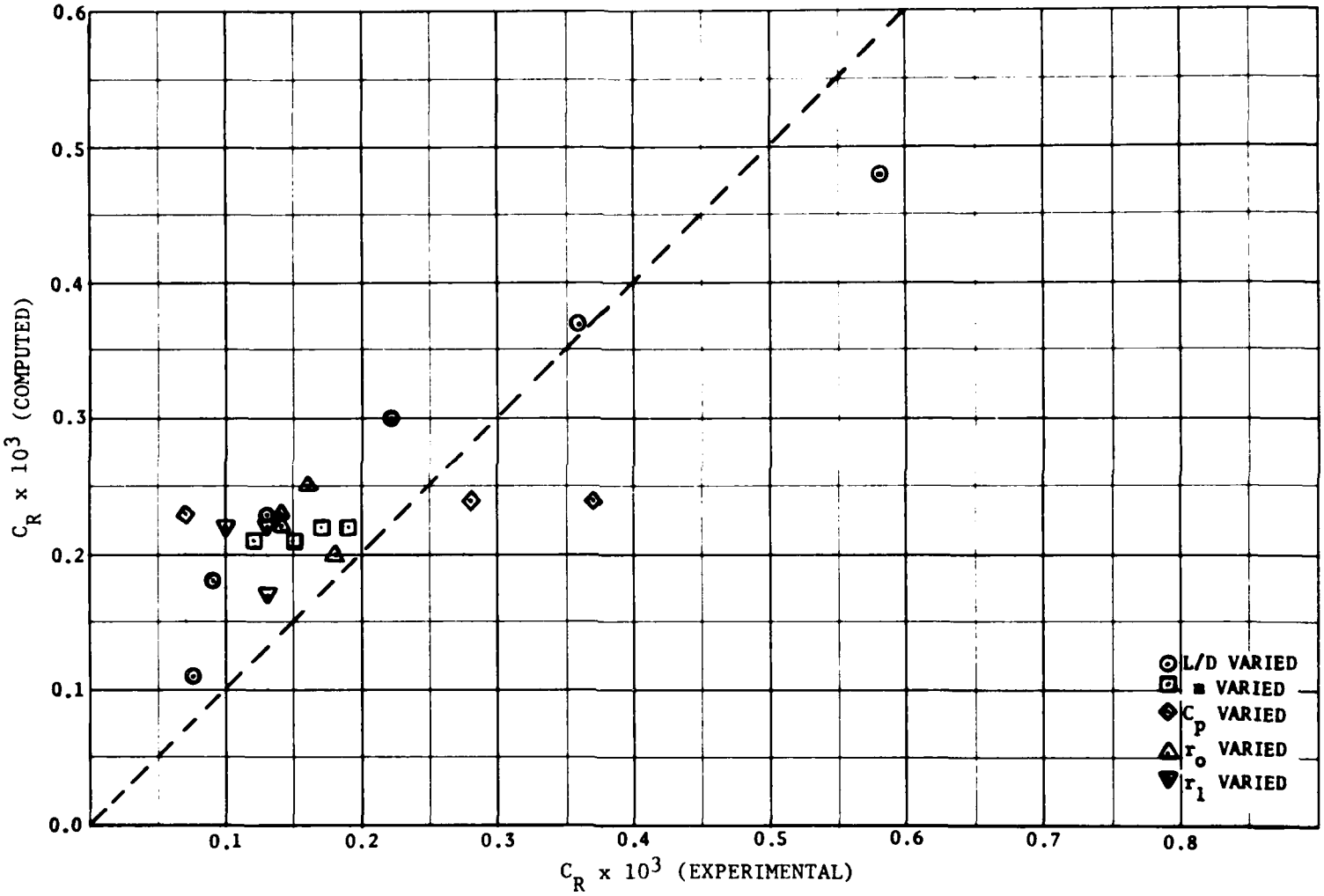

Figure 3 - Comparison of Experimental and Computed C_R Values for Series 58

The computed values of C_R as a function of L/D have the same order of merit as the experimental values shown in Table 2. However, the computed values of C_R listed in Tables 3, 4, 5, and 6 and illustrated in Figure 3, indicate that the simple formula is relatively insensitive to changes in m, C_p, r_o, and r_1. For example, Table 4 shows very little difference in the computed values of C_R as a function of C_p, whereas the experimental data show a strong dependence of C_R on C_p. Figure 3 shows that except for three models the experimental values of C_R are less than the computed C_R values.

The only series where consistent trends can be seen in both computed and experimental C_R values is for models where L/D varies (Table 2). Both experimental and computed C_R's show decreasing C_R with increasing L/D. Both the experimental data and the simple formula were able to discriminate the three worst bodies of this series; thus, it is possible that the formula may be used to identify a really poor body when L/D is being varied, but not necessarily for variations of other geometric parameters.

Models 5242-1, 2, 3

The second series of bodies investigated was the Series 5242 models. These bodies have identical forebodies with sterns of differing fullness. The amount of parallel middle body on each model was varied to produce three models of essentially constant volume. Figure 4 shows sketches of three full-scale hulls with changes in length due to the constant-volume constraint. For the present study, the hulls were treated as bodies of revolution without appendages.

Scaled offsets were taken from the drawings and polynomials were passed through the offset points to form a smooth fit. The three tails were described by quartics of the form

$$y = A x^4 + B x^3 + C x^2 + D x$$

The common nose for the three models was described similarly but using a quadratic fit. Direct use of scaled offsets was also tried but the rate of change of curvature was not smooth enough to avoid fluctuations of the pressure distribution over the body. Final pressure distributions for the 5242 series can be found in Figure 8A of Appendix A. Table 7 shows

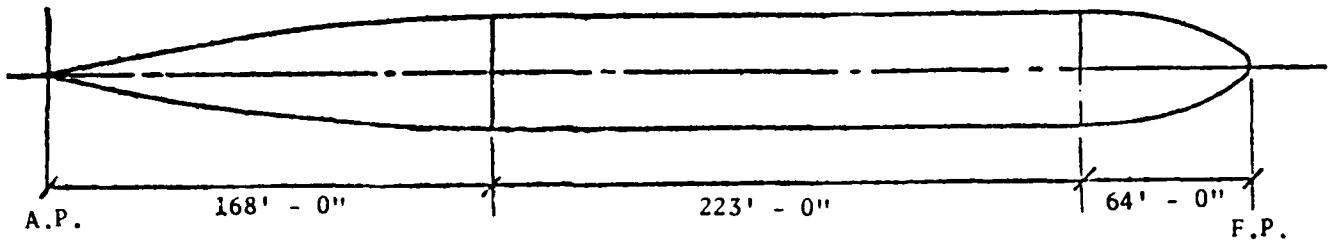

5242-3 $L_R/D=4$

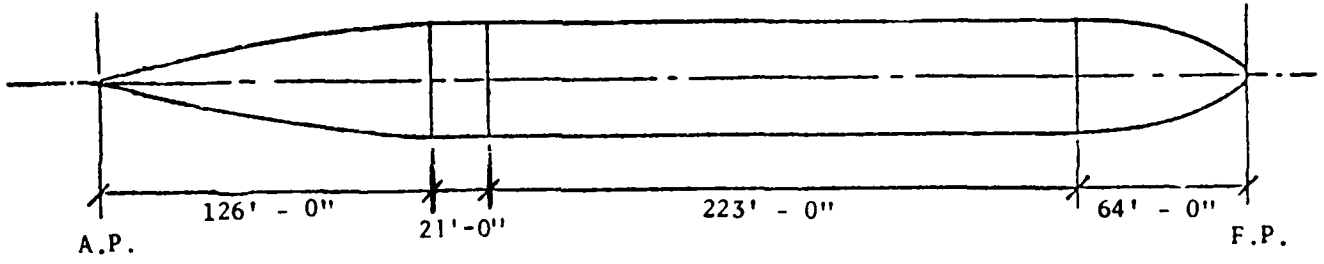

5242-2 $L_R/D=3$

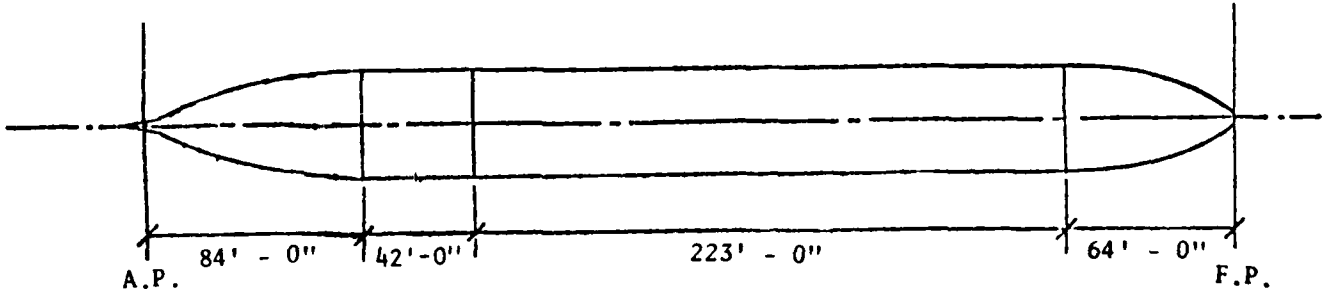

5242-1 $L_R/D=2$

Figure 4 - Configurations Represented by Models 5242-3, 5242-2, and 5242-1

experimental results for the Series 5252 models along with the computed values of C_R/C_f and the value of C_R calculated at a Reynolds number of 20×10^6. Figure 5 shows a graphical comparison between the computed and experimental values of C_R.

TABLE 7

Residual Drag Comparisons for the Series 5242 Models

Model	$C_{p_{stern}}$	L_R/D	Experimental $C_R \times 10^3$	Calculated C_R/C_f Simple Formula	Calculated $C_R \times 10^{3*}$
5252-1	0.674	2	0.375	0.88	0.23
5242-2	0.574	3	0.310	0.076	0.20
5242-3	0.505	4	0.255	0.079	0.21

*Based on $Rn_L = 20 \times 10^6$ (16)

The bare-hull data show that C_R increases with decreasing L_R/D; Model 5252-3 with $L_R/D = 4$ is the best in the series. The simple formula, however, predicts that Model 5252-2 with $L_R/D = 3$ is the best model. Thus, the experimental and computed results are not in agreement for these bodies. Figure 5 shows that the predicted drag is not very sensitive to change of the parameter L_R/D. The predicted values of C_R are lower than the measured values of C_R, which was not true for the Series 58.

Kempf Sterns

The third series studied consisted of six bodies of revolution having hemispherical noses and sinusoidal sterns of varying fullnesses. These sterns were investigated initially by G. Kempf.[11,12] The models were 4 meters in length and consisted of 0.3 meter diameter pipe 3.1 meters long, with 0.9 meter afterbodies described by sinusoids having different wavelengths. Sketches of the sterns are shown in Figure 6.

The point generation program used the following equation for each of the stern sections

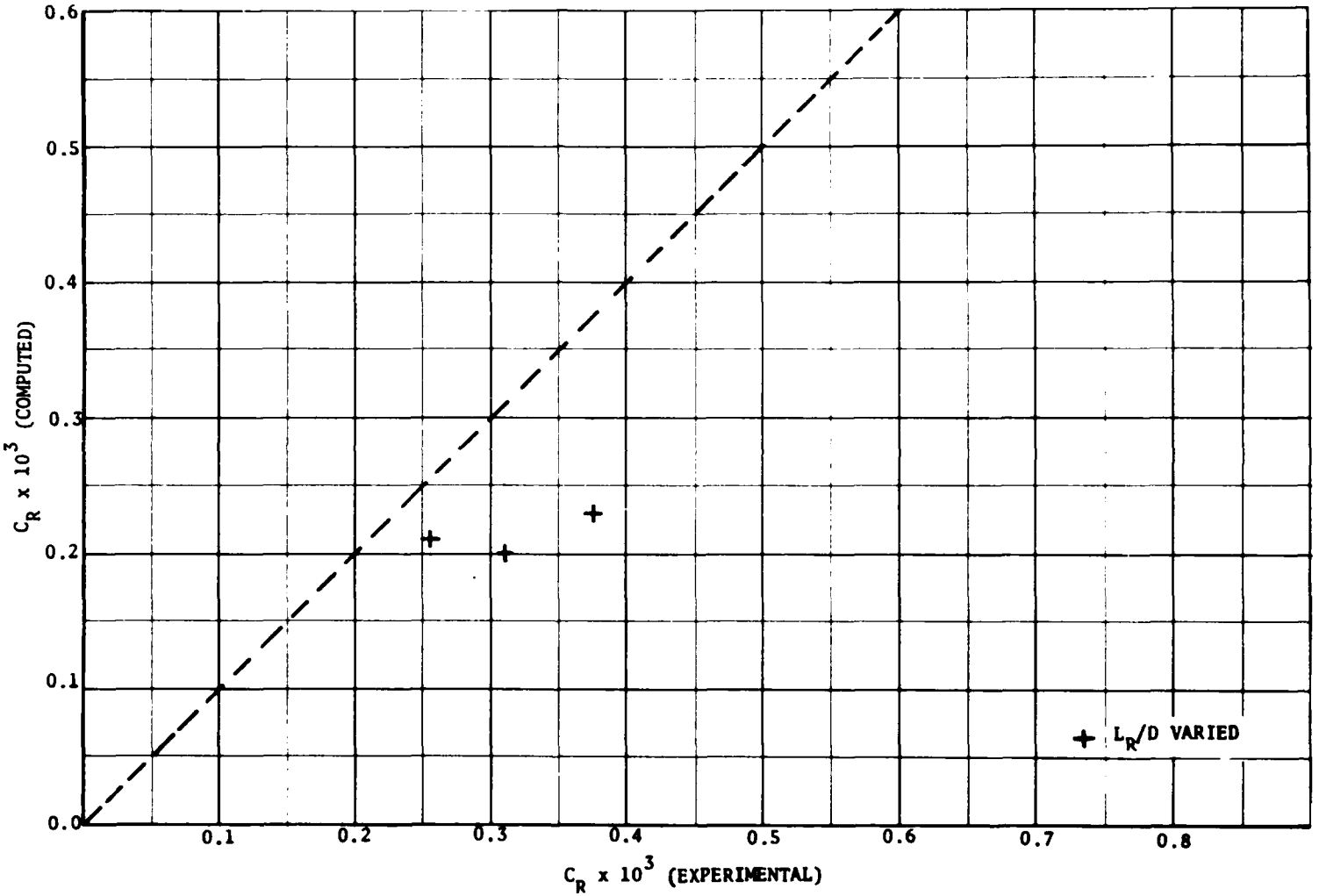

Figure 5 - Comparison of Experimental and Computed C_R's for the Model Series 5242

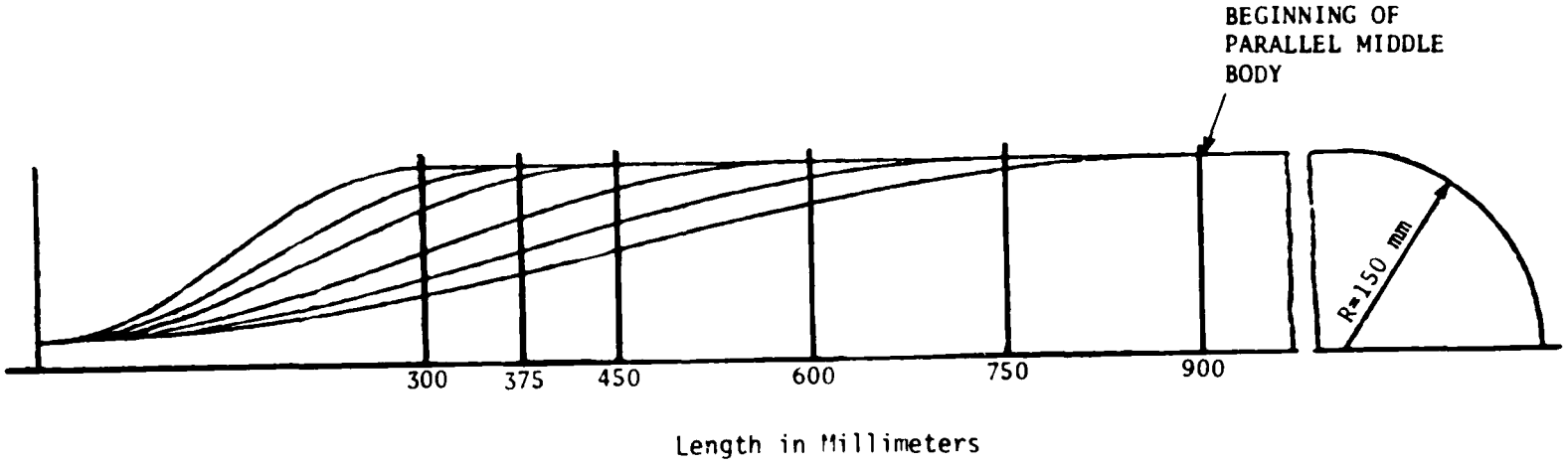

Figure 6 - Kempf Body Configurations

$$r = \sin\theta = \sin\frac{\pi\bar{x}}{2L_R}$$

where $0 < \theta < \frac{\pi}{2}$,

$\bar{x}$ is measured from the aft perpendicular, and

L_R is the length of the rear section.

The tail radius of these bodies is not zero at the aft perpendicular, but has a value of 37 mm. To minimize possible and effects on the pressure calculations, an imaginary section of 0.9 meter length and 37 mm radius was added to the body points generated analytically (see Figure 7). Calculations from direct offsets were also tried but the rate of change in r was not smooth enough to prevent severe fluctuations in C_p.

Computations of the integral in equation [20] were carried out only to the end of the actual body and not to the end of the imaginary extension. Computed and measured drag values are shown in Table 8, a graphical comparison of C_R's based on a model scale Reynolds number of 20×10^6 is shown in Figure 8, and final pressure distributions may be founded in Figure 9A of Appendix A.

TABLE 8

Residual Drag Comparisons for Kempf Body Series

Model	L_R/D	Experimental $C_R \times 10^3$	Computed C_R/C_f Simple Formula	Computed $C_R \times 10^{3*}$ Simple Formula
I	3.0	0.07	0.76	0.20
II	2.5	0.14	0.76	0.20
III	2.0	0.20	0.78	0.21
IV	1.5	0.30	0.081	0.21
V	1.25	0.42	0.099	0.26
VI	1.00	0.75	0.089	0.23

*Based on $Rn_L = 20 \times 10^6$ (16)

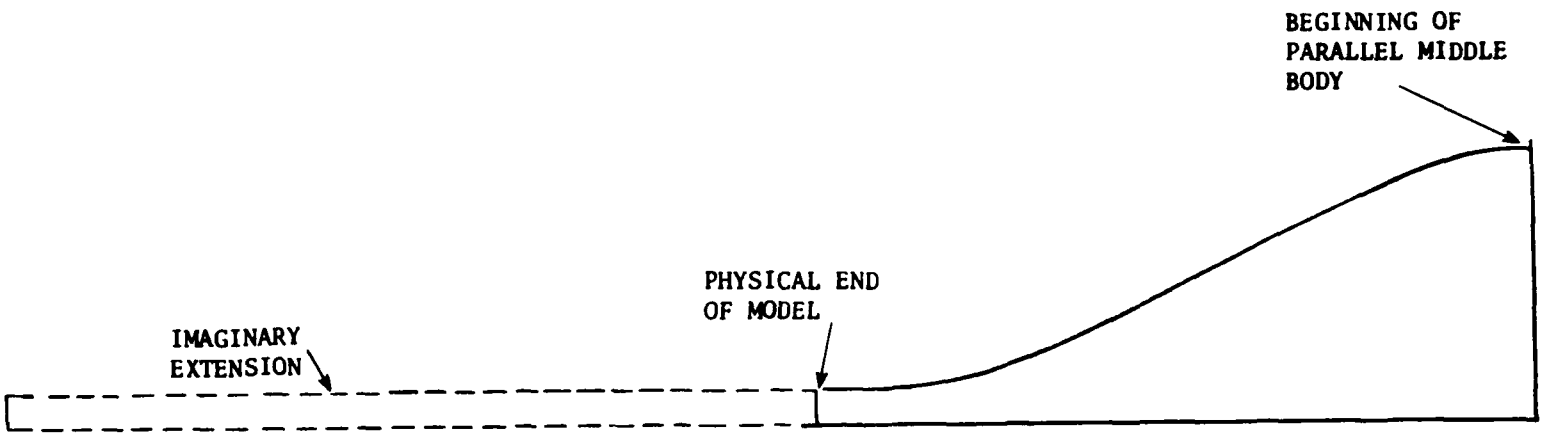

Figure 7 - Sketch of Imaginary Tail Extension Used for Potential Flow Calculations to Minimize End Effects on Kempf Bodies

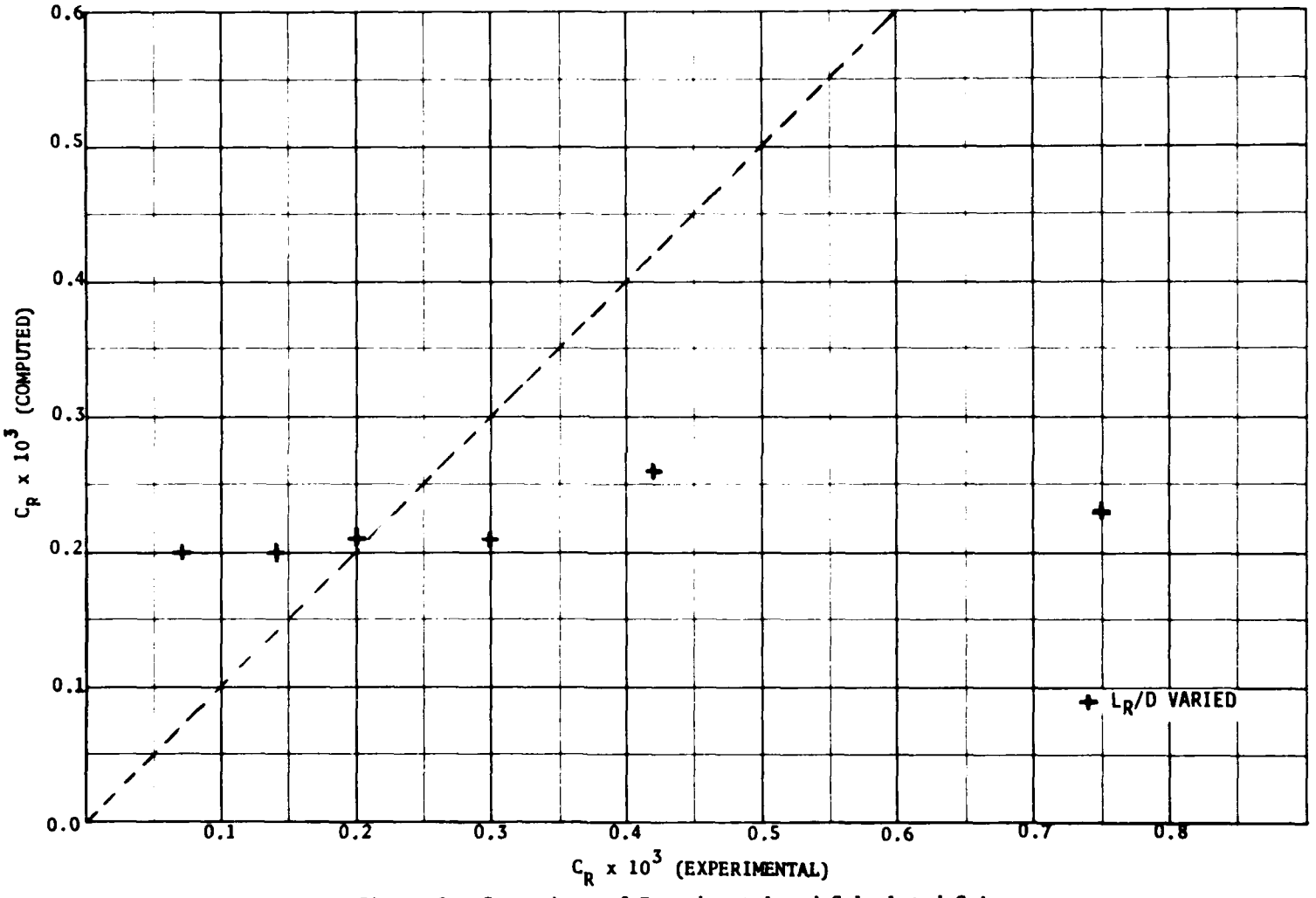

Figure 8 - Comparison of Experimental and Calculated C_R's for Kempf Series Bodies

The experimental results given by Kempf show a consistent increase in C_R with decreasing L_R/D. With the exception of Model VI, the simple formula also shows this trend, although not differentiating nearly as strongly between models as the experimental values. Model VI surely has extensive separation which would invalidate the simple formula, since it requires an unseparated boundary layer. As Figure 8 shows, the simple formula does not adequately predict the very large experimental increase of C_R values with decreasing stern fineness, L_R/D.

Parallel Middle Body Series

The fourth series of body models studied was based on the experimentally-determined "best" model of Series 58 (Model 4165). The original equation

$$y^2 = a_1x + a_2x^2 + a_3x^3 + a_4x^4 + a_5x^5 + a_6x^6$$

with

$a_1 = 1.0$
$a_2 = 0.837153$
$a_3 = -8.585996$
$a_4 = 14.075954$
$a_5 = -10.542535$
$a_6 = 3.215422$

was used for the nose and tail with increasing amounts of parallel middle body added to generate a new series of models. The experimental series, as reported by Larsen,[13] gives data for models having 30, 40, 50, and 60 percent of their lengths in parallel-middle-body.

Sketches of the models are shown in Figure 9, computed pressure distributions are given in Figure 10A of Appendix A, and results of the drag calculations are listed in Table 9. Calculated values of C_R are based on a model Reynolds number of 20×10^6, using C_f values calculated from the Schoenherr formula.[16] Figure 10 gives a graphical comparison of the computed and experimental values of C_R.

[16] Schoenherr, K.E., "Resistance of Flat Surfaces Moving Through a Fluid," Transactions, Society of Naval Architects and Marine Engineers, Vol. 40 (1932).

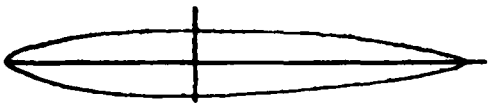

Model 4165

L/D = 7.00

$m = 0.40$

$r_o = 0.50$

$r_1 = 0.10$

$c_p = 0.60$

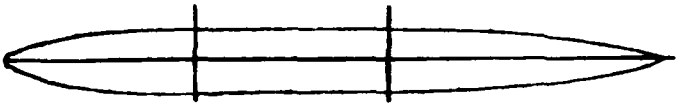

Model 4165-30

30% PMB L/D = 10.00

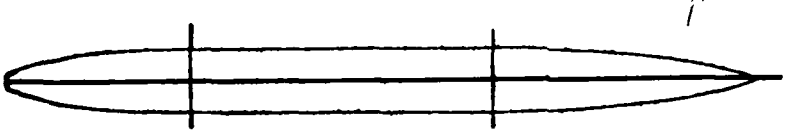

Model 4165-40

40% PMB L/D = 11.67

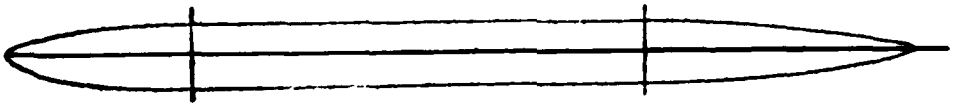

Model 4165-50

50% PMB L/D = 14.00

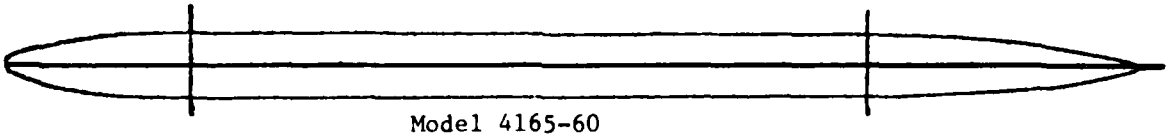

Model 4165-60

60% PMB L/D = 17.50

Figure 9 - Series 58 Model 4165 with Parallel Middle Body

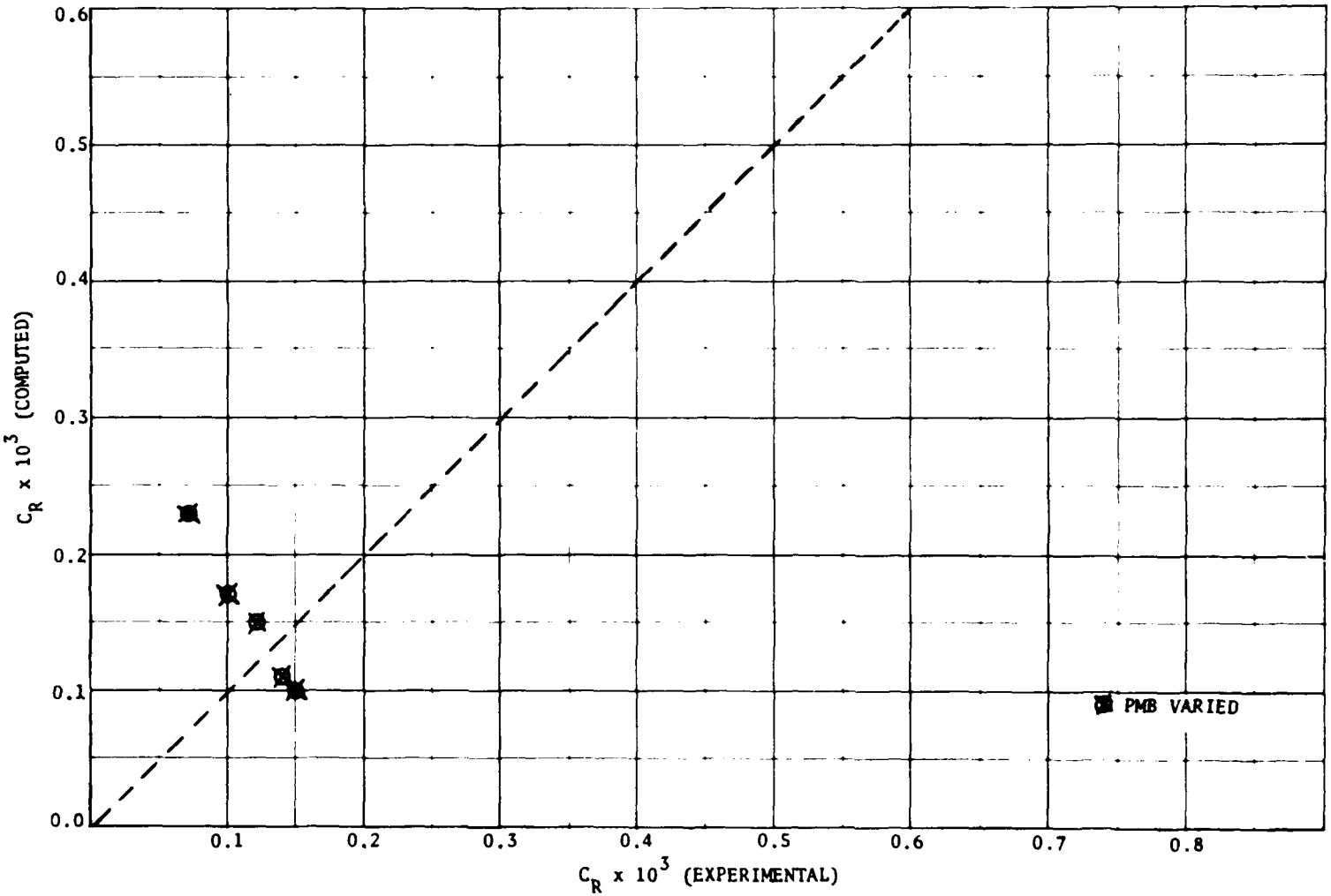

Figure 10 - Comparison of Experimental and Calculated C_R's for the Series 58 Parallel Middle Body Models

TABLE 9

Residual Drag Comparisons for the Series 58 Parallel Middle Body Series
(Nose and tail shape fixed, maximum diameter fixed)

Model	L/D	Experimental $C_R \times 10^3$	Calculated C_R/C_f Simple Formula	Calculated $C_R \times 10^{3*}$ Simple Formula
4165	7.00	0.07	0.088	0.23
4165-30	10.00	0.10	0.064	0.17
4165-40	11.67	0.12	0.055	0.15
4165-50	14.00	0.14	0.045	0.12
4165-60	17.50	0.15	0.037	0.10

*C_F computed at $Rn_L = 20 \times 10^6$. (16)

The experimental data of Figure 10 show that C_R values increase with increasing amounts of parallel middle body. The simple formula shows values of C_R decreasing with increasing parallel middle body. This trend in the computed drags is consistent with the Series 58 data which showed a similar reduction in the values of C_R with increasing L/D. It is in disagreement with Larsen's experimental data illustrated in Figure 10.

If one considers a form of fixed nose and tail shape and fixed maximum diameter being elongated by increasing amounts of parallel middle body, it would be reasonable to expect a thicker stern boundary layer and possibly larger values of the residual (or form) drag due to an increasing pressure defect at the stern. However, a comparison of the relative computed form drags, given by the product $S \cdot C_R$, where S is the wetted surface area, revealed the same trends as given by the values of C_R shown in Table 9 and Figure 10.

Model 4620-1, 2, 3, 4 Forebody Series

The fifth series of bodies studied was initially investigated by McCarthy, Power, and Huang,[14] and will be designated Series 4620 after the parent model. The parent model provided the common tail form for the series. The series is comprised of four bodies of revolution having bow entrance-length/diameter ratios (L_E/D) of 0.5, 1.0, 1.82, and 3.0. Each forebody has a prismatic ratio C_{P_E} of 0.667. The bluntest fore-body ($L_E/D = 0.5$) has a hemispherical nose. The other three forebodies are described by Granville polynomials which provide a smooth junction with the parallel middle bodies.[17] These polynomials are defined by the expression:

$$y^2 = .833\ R(x) + 10\ \bar{K}_1(x) + Q(x)$$

where $y = 2Y/D$

$x = X/L$

D = maximum diameter

L = body length

x, y = dimensional *body points*

and

$$R(x) = 2\ x\ (x-1)^4$$
$$\bar{K}_1(x) = 1/3\ x^2\ (x-1)^3$$
$$Q(x) = 1 - (x-1)^4\ (4\ x + 1)$$

For the series, the total model hull volume was held constant by varying the length of parallel middle body. Sketches of the bodies are shown in Figure 11 and pressure distributions for the series are given in Figure 11A of Appendix A. The comparisons between the experimental C_R data and the computed values of C_R/C_f are shown below in Table 10, and a graphical comparison of computed and experimental C_R's is shown in Figure 12. Computed C_R's are based on a model Reynolds number of 20×10^6.

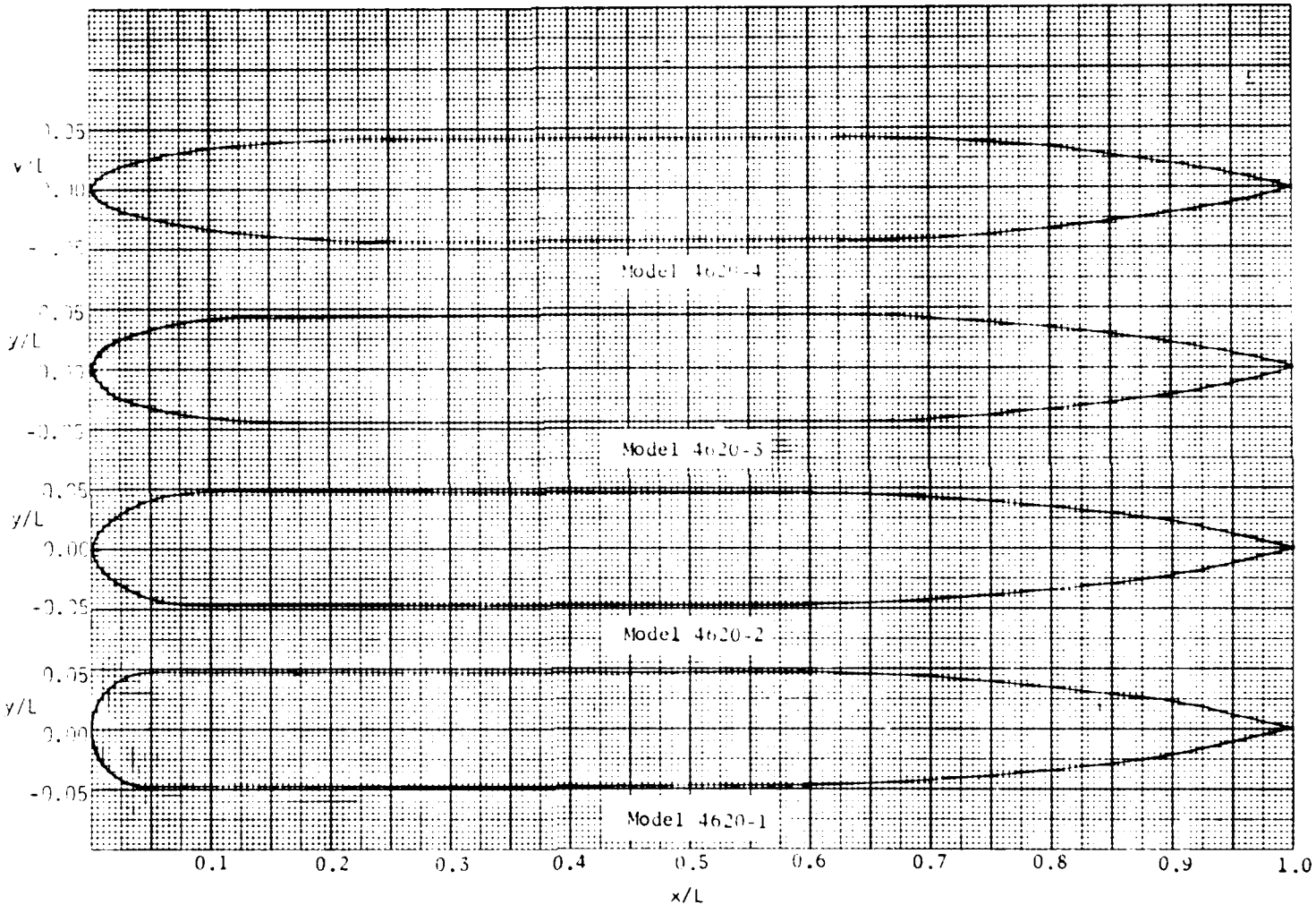

Figure 11 - Nondimensional Plot (x/L, y/L) of Series 4620-1, 2, 3, 4, Models

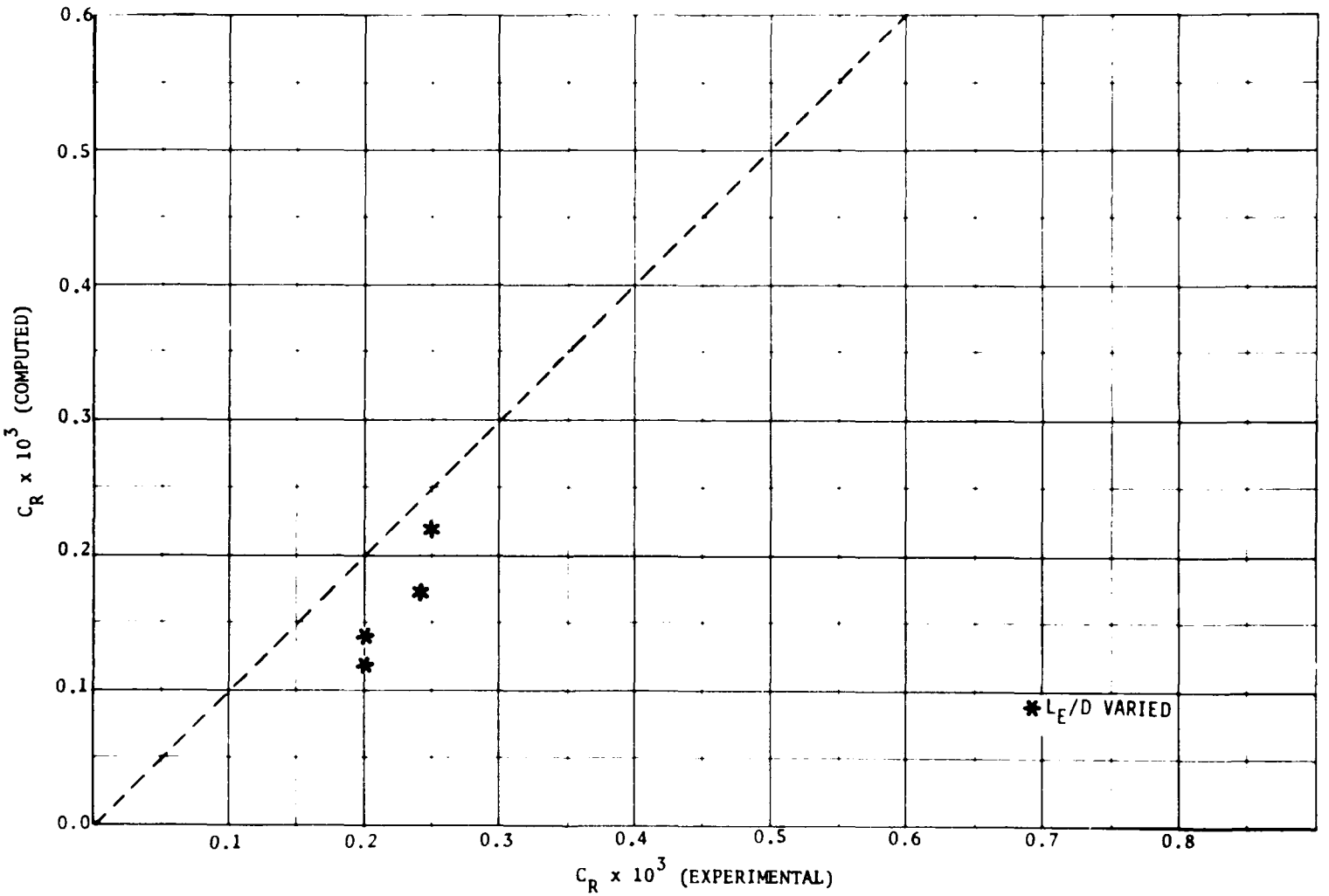

Figure 12 - Comparison of Experimental and Calculated C_R's for Model Series 4620-1, 2, 3, 4

TABLE 10

Residual Drag Comparisons for Series 4620-1, 2, 3, 4

Model	L_E/D	Experimental $C_R \times 10^3$	Computed C_R/C_f Simple Formula	Computed $C_R \times 10^{3*}$ Simple Formula
4620-1	0.50	0.25	0.084	0.22
4620-2	1.00	0.24	0.063	0.17
4620-3	1.82	0.20	0.052	0.14
4620-4	3.00	0.20	0.047	0.12

*Based on C_f computed at $Rn_L = 20 \times 10^6$. (16)

Both the measured and predicted values of drag show the same relative order of merit for this series. The values of C_R increase with decreasing L_E/D. However, the simple formula predicts lower values and a greater spread between the values of C_R for the four models.

OTHER HULL MODELS

A sixth group consisting of miscellaneous model hulls fitted with polynomials was investigated. Five models were involved: Model 4620, Model 4935, Model 4627, Model 5224-1, and Model 5290. Four of the five models were fitted with Granville polynomials. Models 4935, 5290 and 5224-1 were fitted using Granville[17] equations for parallel-middle-body models. Model 4627 was fitted using Granville[18] equations for forms without parallel middle body. Model 4620 was fitted with a polynomial of Series 58 form, $Y^2 = a_1 X + a_2 X^2 + a_3 X^3 + a_4 X^4 + a_5 X^5 + a_6 X^6$ where, $X = x/L$ and $Y = y/D$. The least squares fit provided by these polynomials was shown to be necessary to remove irregularities from drawing offsets and to provide a smooth distribution in C_p. The agreement with the offsets was fairly good. It should be noted that Model 4620 is an original parent form without parallel middle body. The 4620-1, 2, 3, 4 Model Series mentioned previously used the tail for this model but added extensive lengths of parallel middle body. Thus, computations for the parent model are not directly comparable to those for the 4620-1, 2, 3, 4 Series.

Sketches of these model forms are not included here, but their pressure distributions are shown in Figure 12A of Appendix A. A comparison of the predicted and measured drags for this series is shown in Table 11, and a graphical comparison of the C_R's based on a Reynolds number of 20×10^6 is shown in Figure 13.

TABLE 11

Residual Drag Comparisons for Miscellaneous Model Series

Model	Experimental $C_R \times 10^3$	Computed C_R/C_f Simple Formula	Computed $C_R \times 10^3$* Simple Formula
4620	0.10	0.106	0.28
4935	0.11	0.083	0.22
5290	0.15	0.056	0.15
4627	0.20	0.089	0.23
5224-1	0.26	0.061	0.16

*Based on $Rn_L = 20 \times 10^6$ (16)

The experimental and computed values of C_R do not agree as to the relative order of merit for this group of bodies. Experimentally, Model 4620 was best and Model 5224-1 was the worst. The simple formula predicts that Model 5290 is best and that Model 4620 is worst. It should be recalled that the simple method was unable to handle the overall ordering of Series 58, although in that case, it did correctly predict the worst body, which has not happened here.

EXTENDED STERN MODELS

The last series investigated was based on an existing form represented by Model 4935. For this series, extended tail shapes were developed and faired into the original model. Model 4935 is the original hull form. Model 4935-2 incorporates a 10-foot tail extension faired into the original hull approximately 7.5 stations aft of the parallel middle body. Model 4935-3 incorporates an 18-foot extension also faired into the original hull about

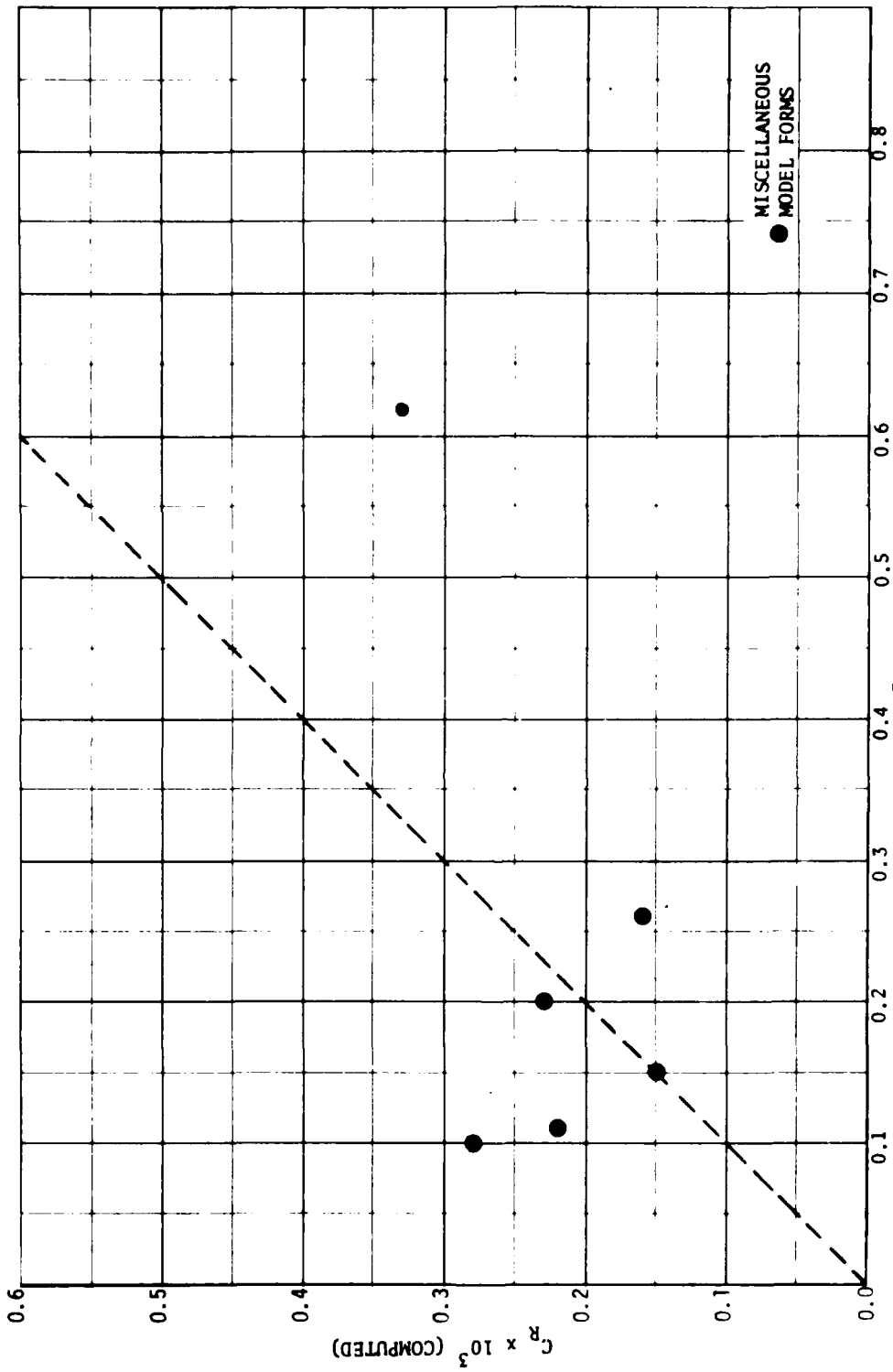

Figure 13 - Comparison of Experimental and Computed C_R's for Miscellaneous Model Forms Series

7.5 stations aft of the parallel middle body. Sketches of the tail forms are shown in Figure 14 and pressure distributions can be found in Figure 13A of Appendix A. Again, a least-squares polynomial fit was used to fair the model offsets in order to obtain pressure and velocity distributions.

Previously unpublished experimental values of C_R are shown in Table 12 along with the C_R's computed from the simple formula. A graphical comparison of the experimental C_R values with computed C_R values based on a model scale Reynolds number of 20×10^6, is shown in Figure 15.

The experimental data show a reduction in the values of C_R with increasing tail length. The simple method predicts that all hulls have nearly the same value of C_R. Thus, the simple method exhibits little sensitivity to changes in L_R/D for these models. The simple method was also not able to predict correctly the drags of the Series 5242 bodies were L_R/D was varied, despite the fact that the L_R/D changes for the Kempf bodies were handled fairly well. The effect of L_R/D on drag apparently cannot be satisfactorily discriminated by the simple formula in all cases.

TABLE 12

Residual Drag Comparisons for Model 4935 Extended Tail Series

Model	Stern Extension (ft)	Experimental $C_R \times 10^3$	Computed C_R/C_f Simple Formula	Computed $C_R \times 10^3$ Simple Formula
4935-1	0	0.23	0.084	0.22
4935-2	10	0.17	0.085	0.22
4935-3	18	0.13	0.082	0.23

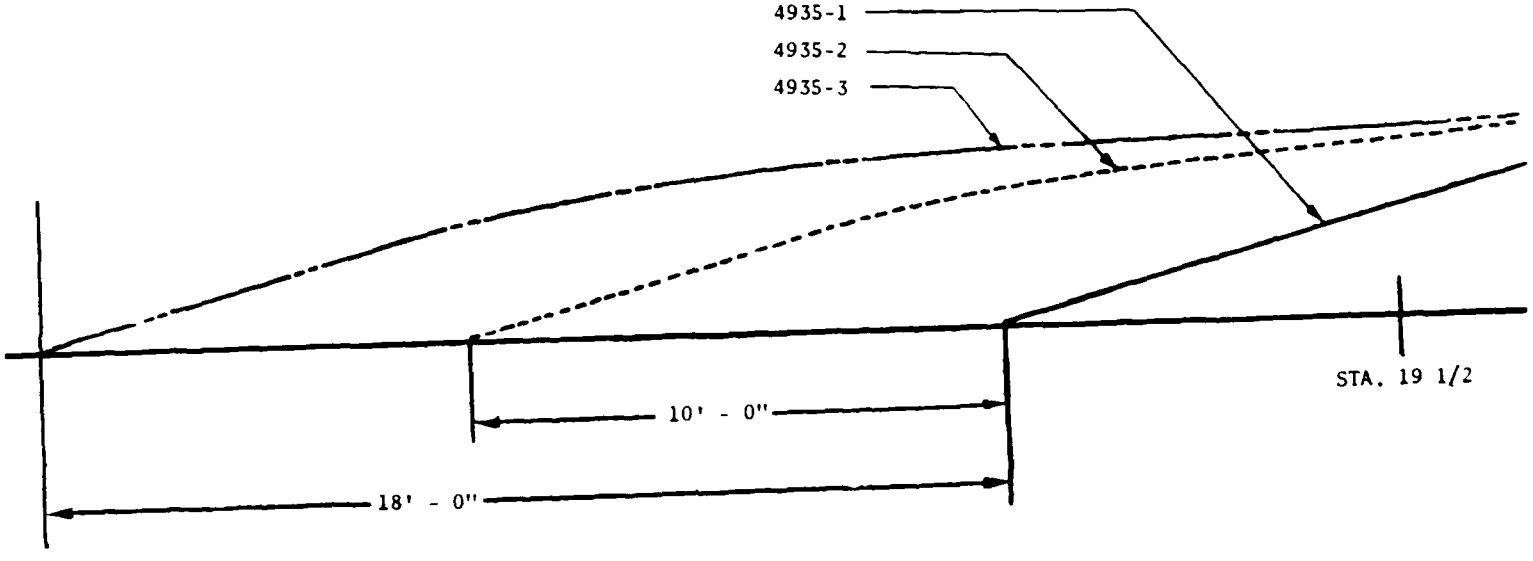

Figure 14 - Model 4935 Extended Tails

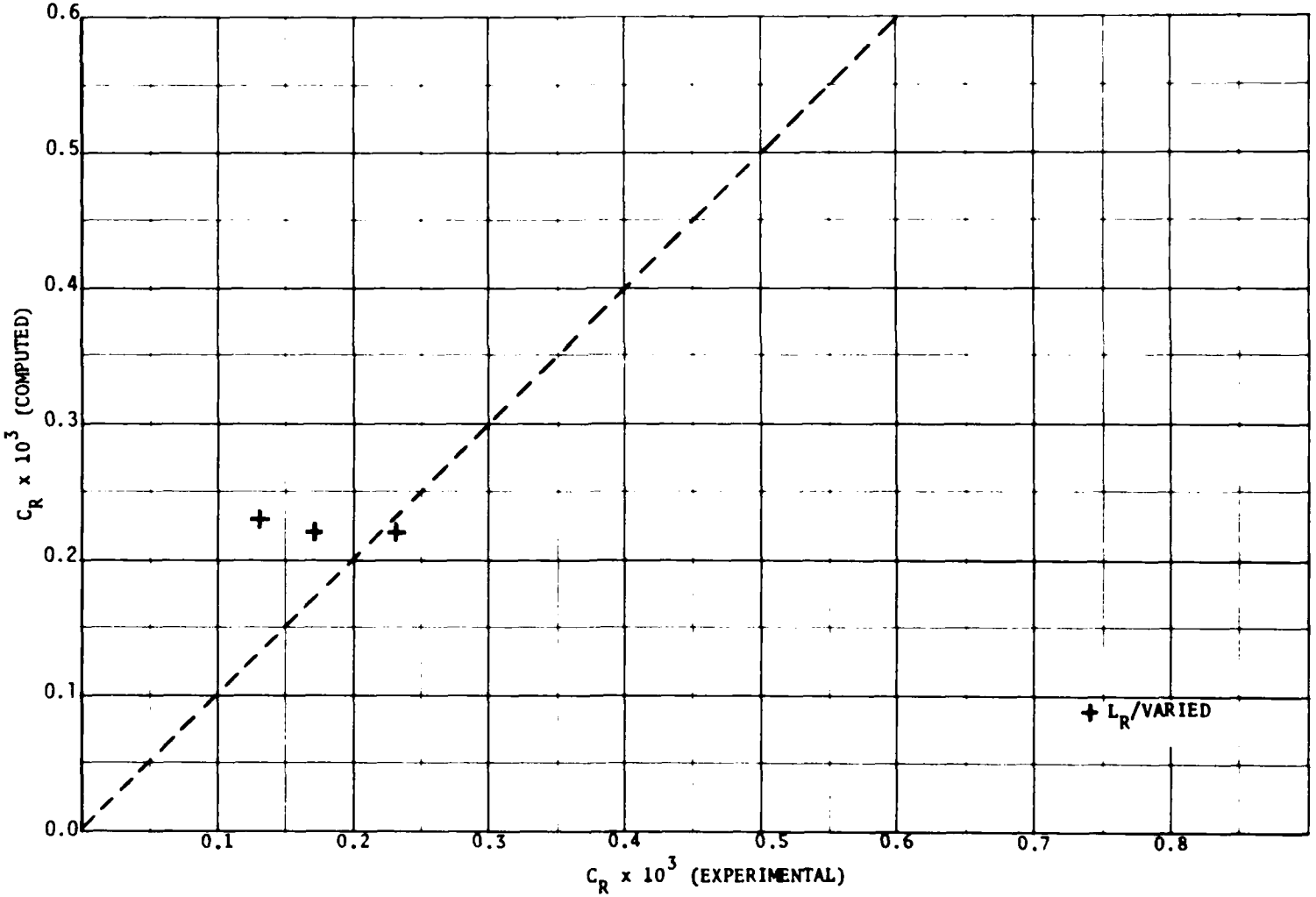

Figure 15 - Comparison of Experimental and Computed C_R's for the Model 4935 Extended Tail Series

CONCLUSIONS

It is apparent that the simplified method has produced mixed results. The computed drags show very little sensitivity to parameters such as C_p, m, r_o, and r_1, as can be seen from the summary graph in Figure 16. Nor does the method appear to be able to discriminate between bodies where many parameters are varied at the same time. In some cases the method does appear to be capable of identifying order of merit when parameters such as L_E/D and L/D are varied. In general, however, the simple formula cannot be recommended for preliminary design or drag evaluation purposes. While the formula does in certain cases predict drag trends which agree with experimental data, it is by no means capable of defining "optimums' and is very likely to be in error for many cases. It is difficult to make these very broad conclusions more precise because of the great scatter in the results and because of the very real possibility that some of the experimental data is incorrect. More detailed conclusions require additional investigations.

ACKNOWLEDGEMENT

The author gratefully acknowledges the assistance of Paul S. Granville, Thomas T. Huang, Keith P. Kerney, and Justin H. McCarthy.

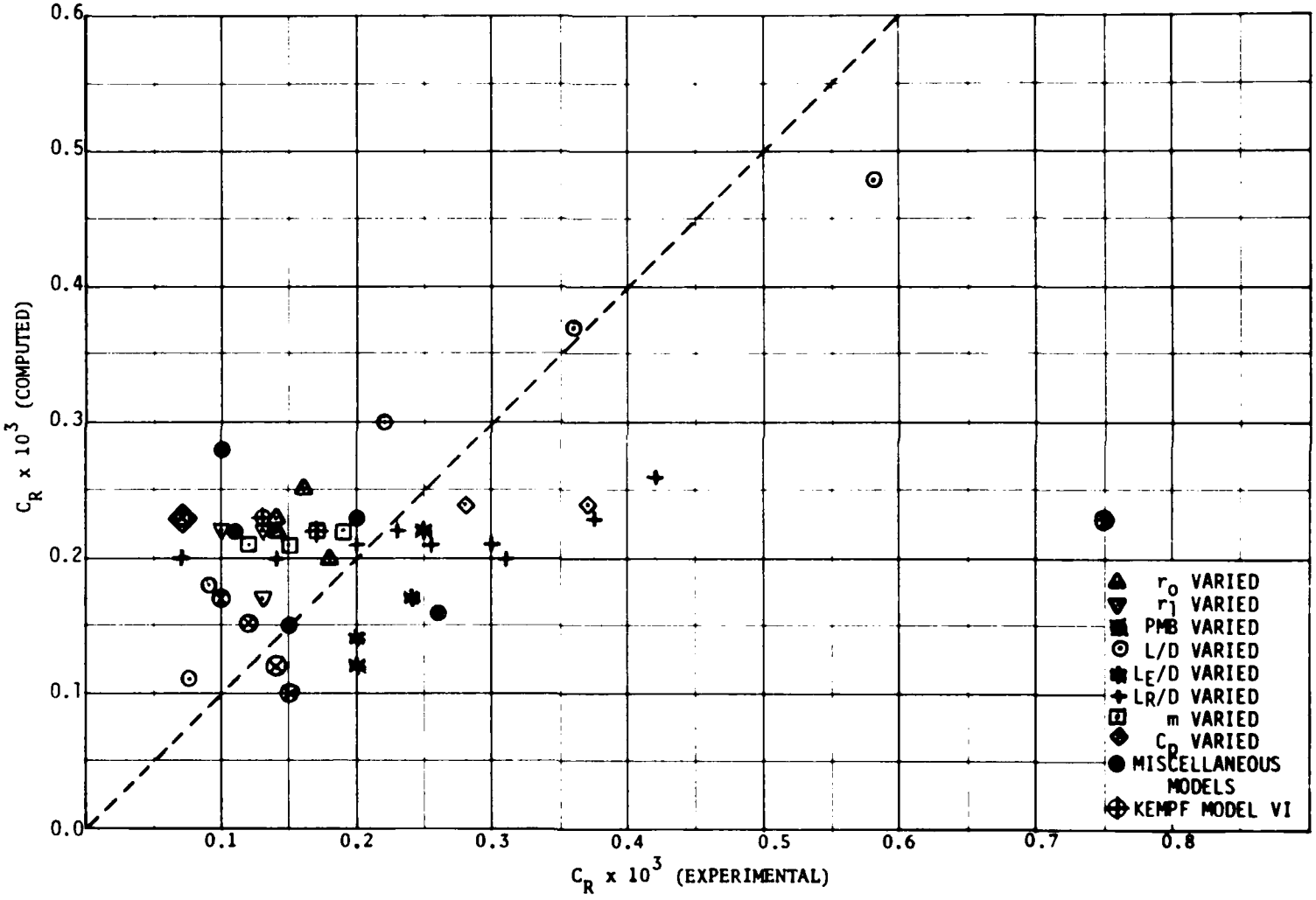

Figure 16 - Summary Comparison for Computed and Experimental C_R's for All Cases

APPENDIX A

PRESSURE DISTRIBUTIONS FOR ALL MODEL FORMS

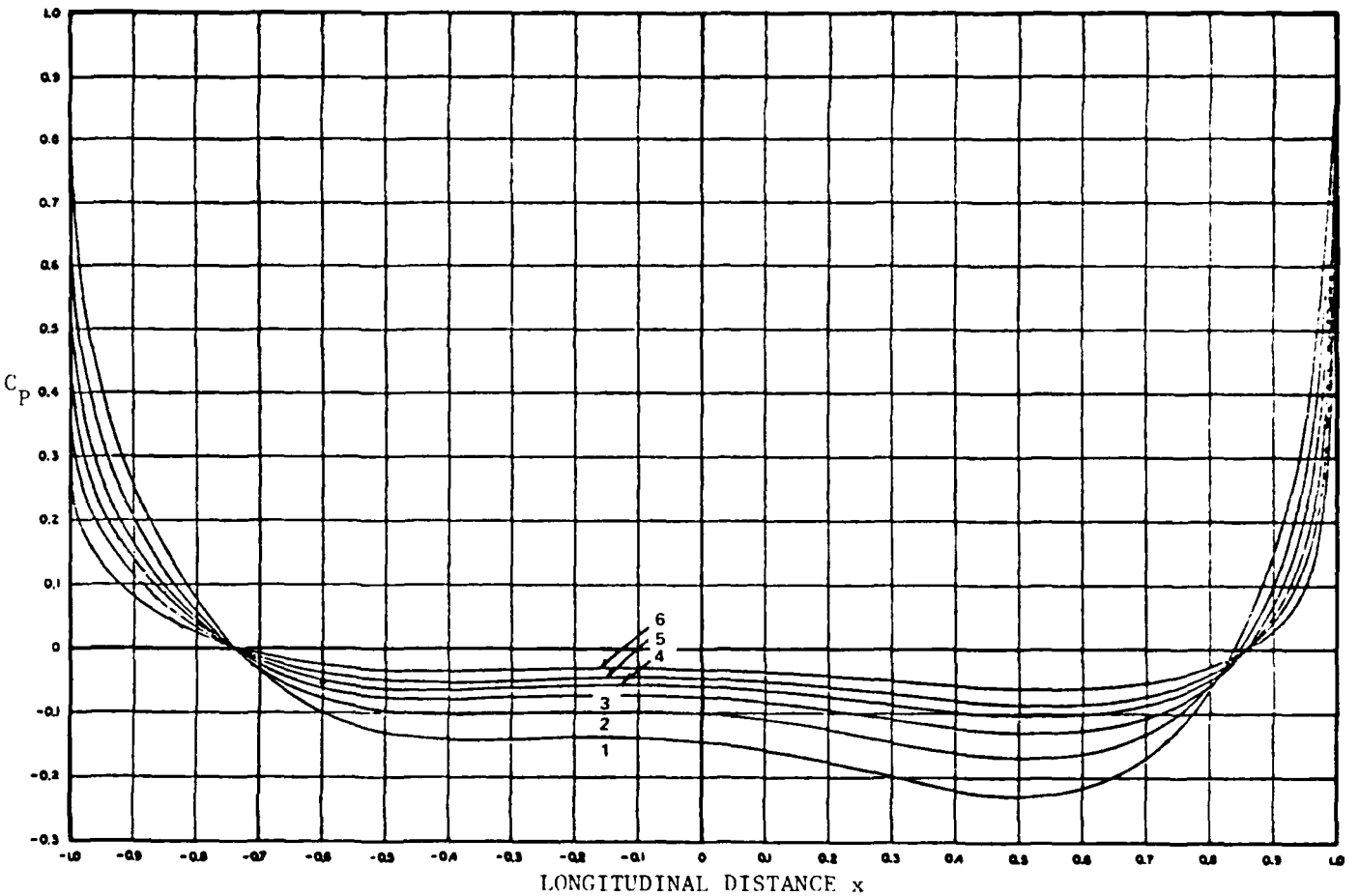

Figure 1A - Pressure Distributions for Longitudinal Flow for Series 58 Bodies with Various Length/Diameter Ratios, $\frac{L}{D}$ (Ref. 15)

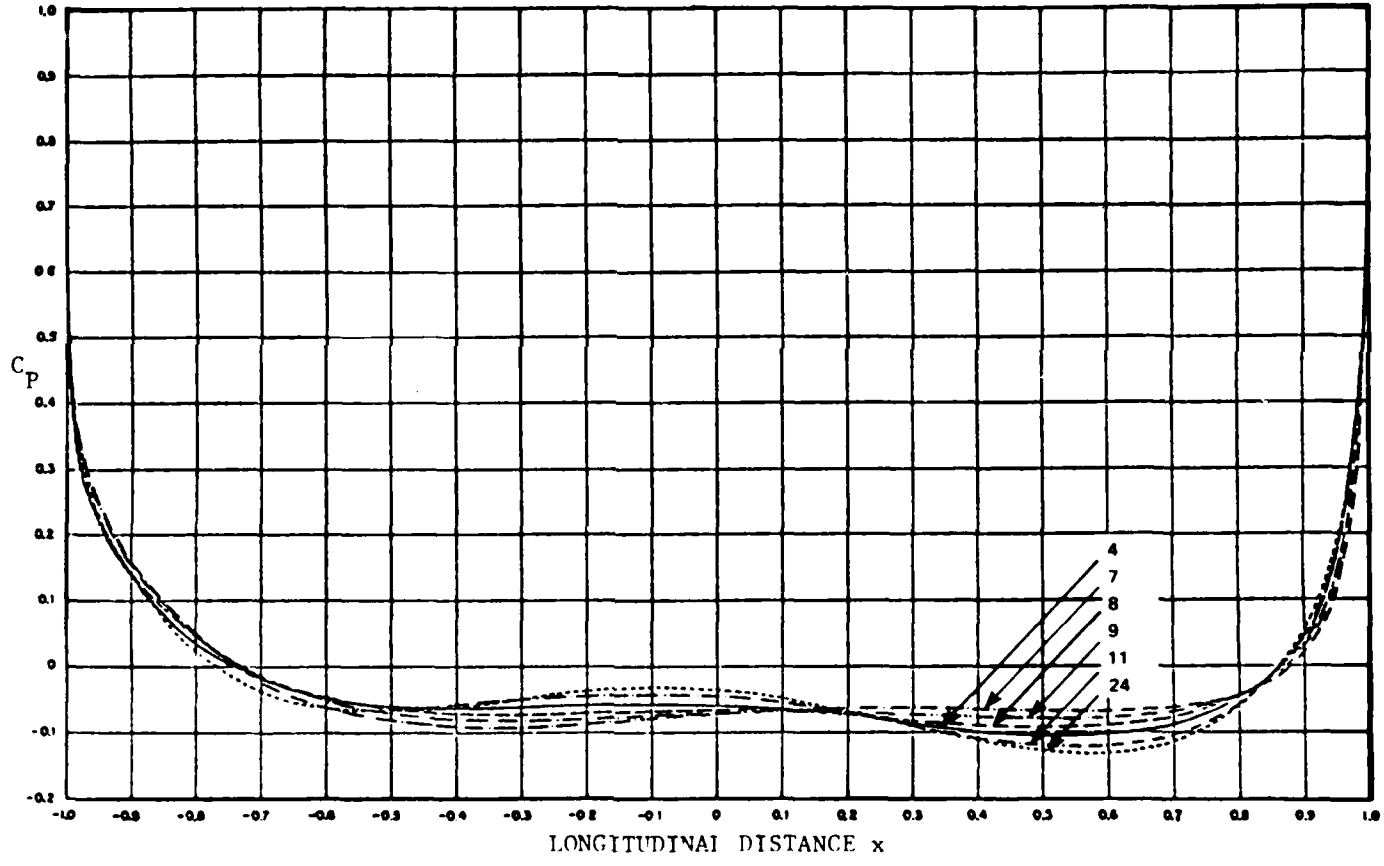

Figure 2A - Pressure Distributions for Longitudinal Flow for Series 58 Bodies with Various Locations of Maximum Section, m (Ref 15.)

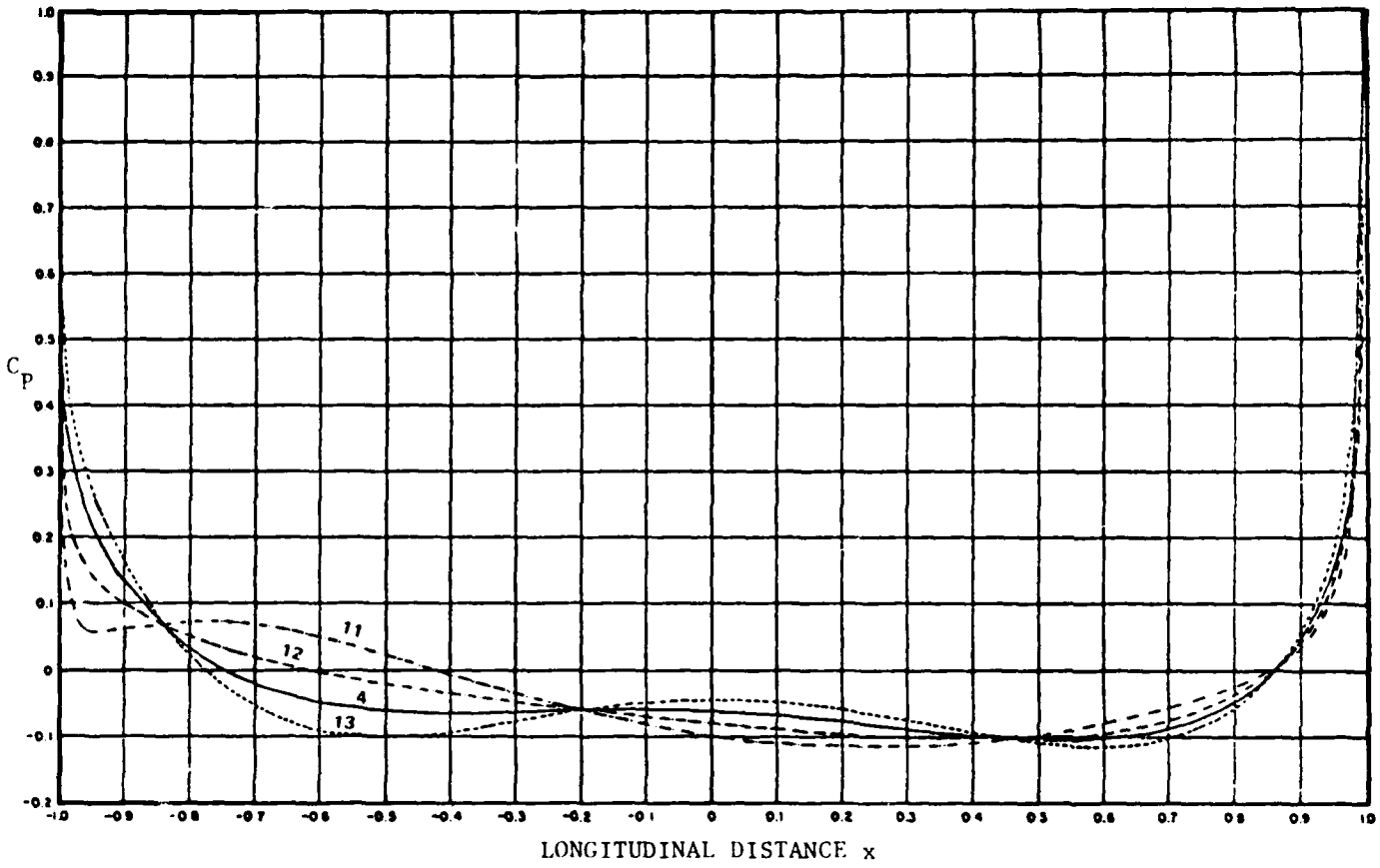

Figure 3A - Pressure Distributions for Longitudinal Flow for Series 58 Bodies with Various Prismatic Coefficients, C_p (Ref. 15)

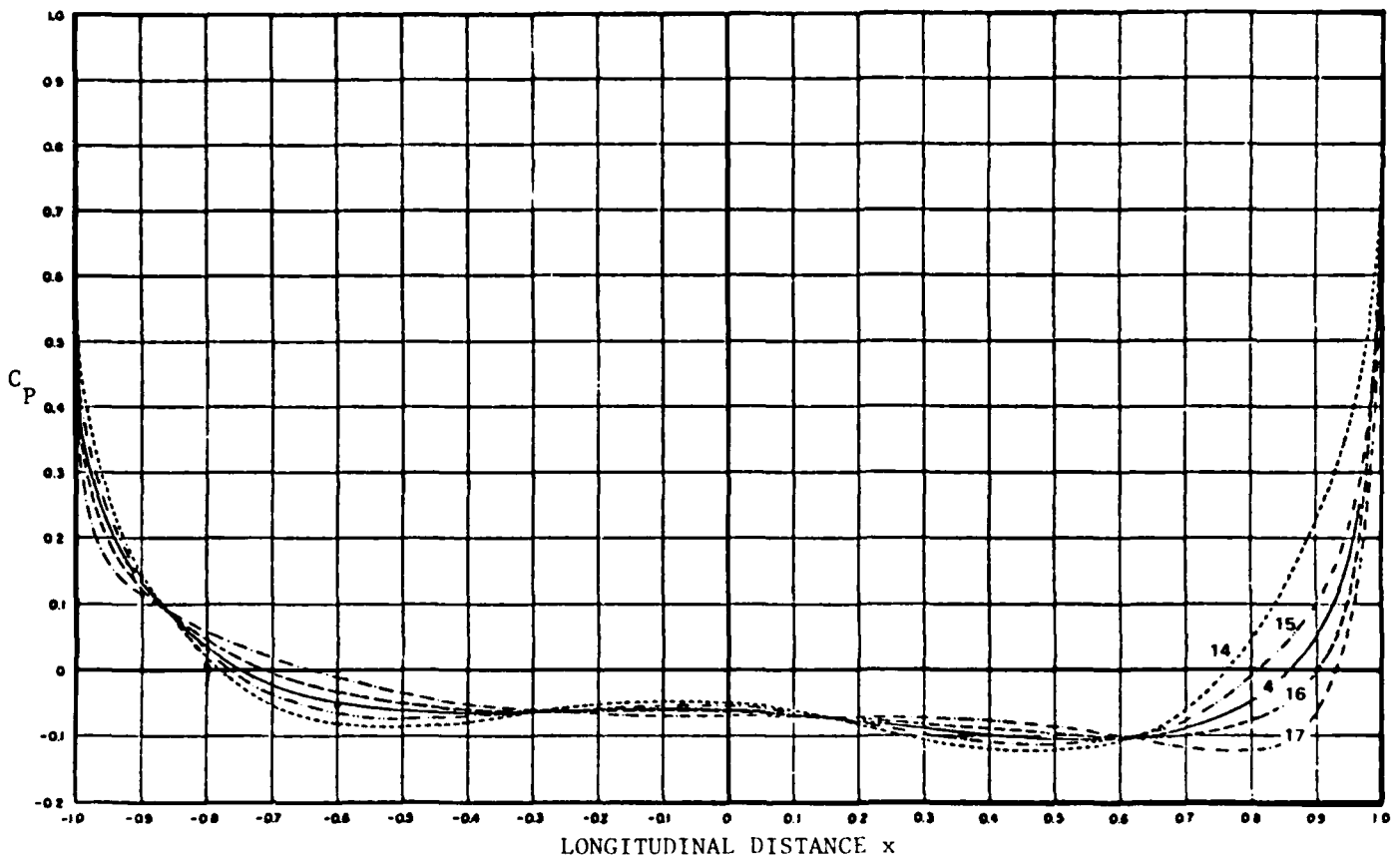

Figure 4A - Pressure Distributions for Longitudinal Flow for Series 58 Bodies with Various Nose Radii, r_o (Ref. 15)

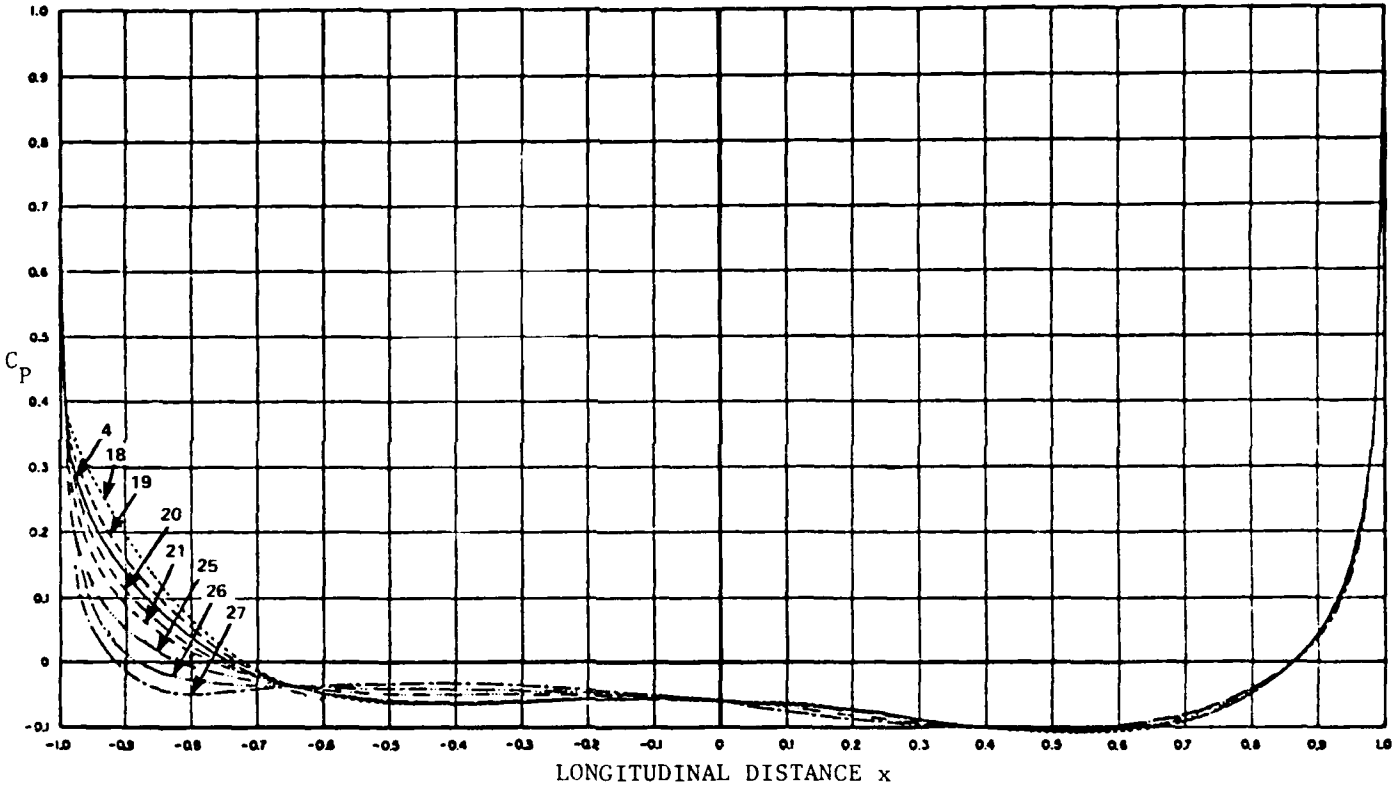

Figure 5A - Pressure Distributions for Longitudinal Flow for Series 58 Bodies with Various Tail Radii, r_1 (Ref.15)

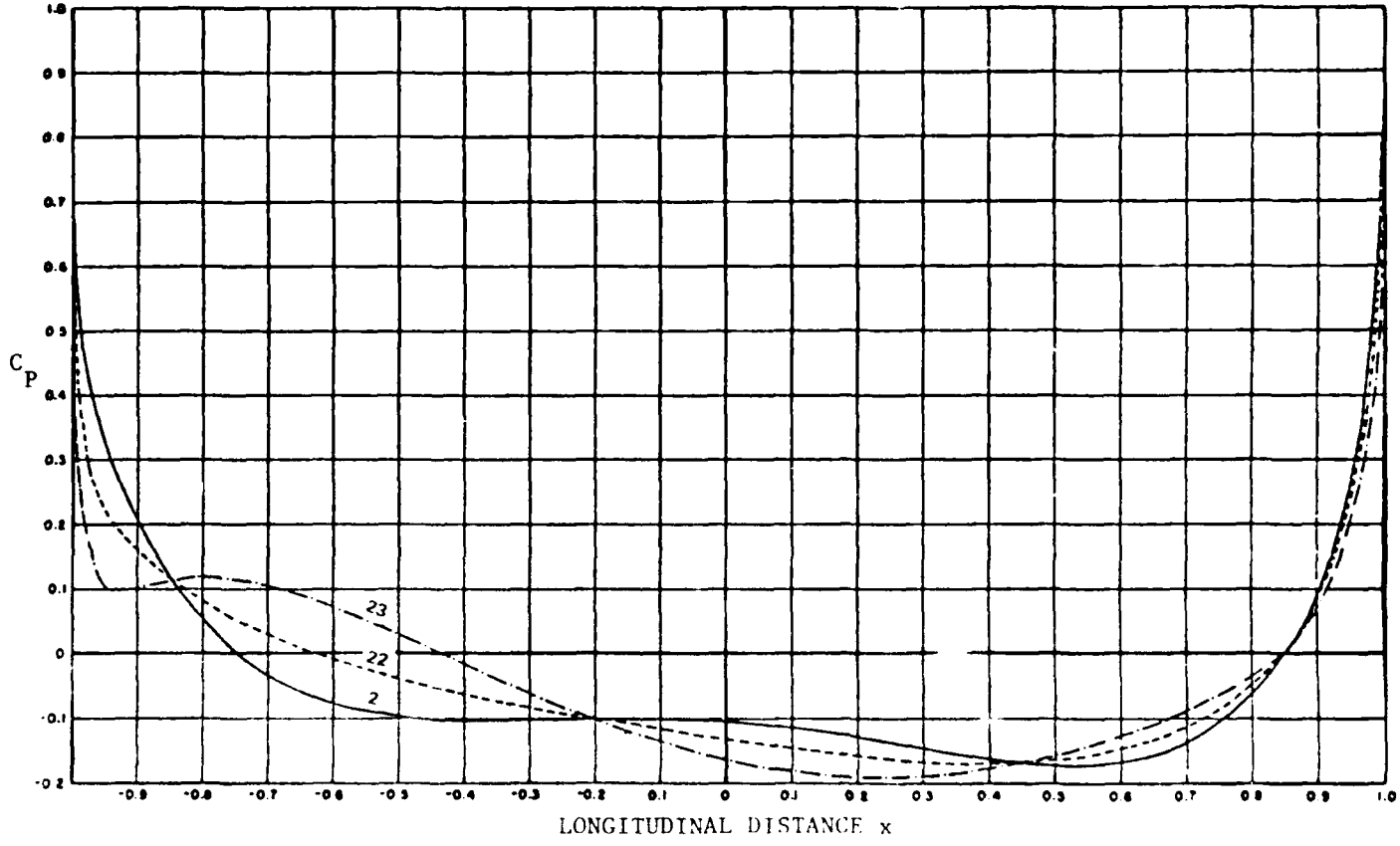

Figure 6A - Pressure Distributions for Longitudinal Flow for Series 58 Bodies with Various Prismatic Coefficients, C_p (Ref. 15)

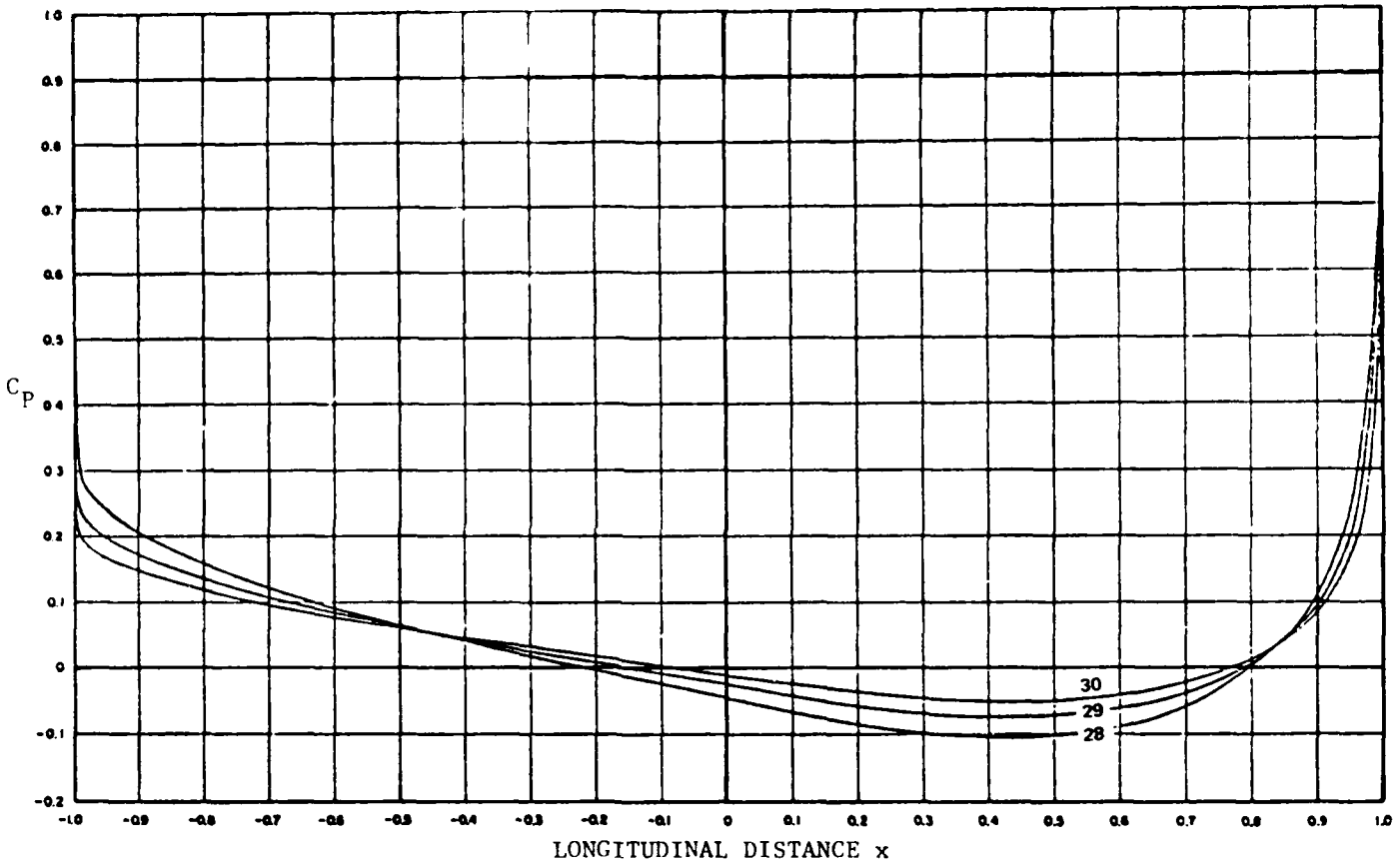

Figure 7A - Pressure Distributions for Longitudinal Flow for Series 58 Bodies with Various Length/Diameter Ratios, L/D (Ref.15)

NOTE: ERRATA SHEET TO REF. 15 STATES TO DECREASE ORDINATE SCALE BY 0.05

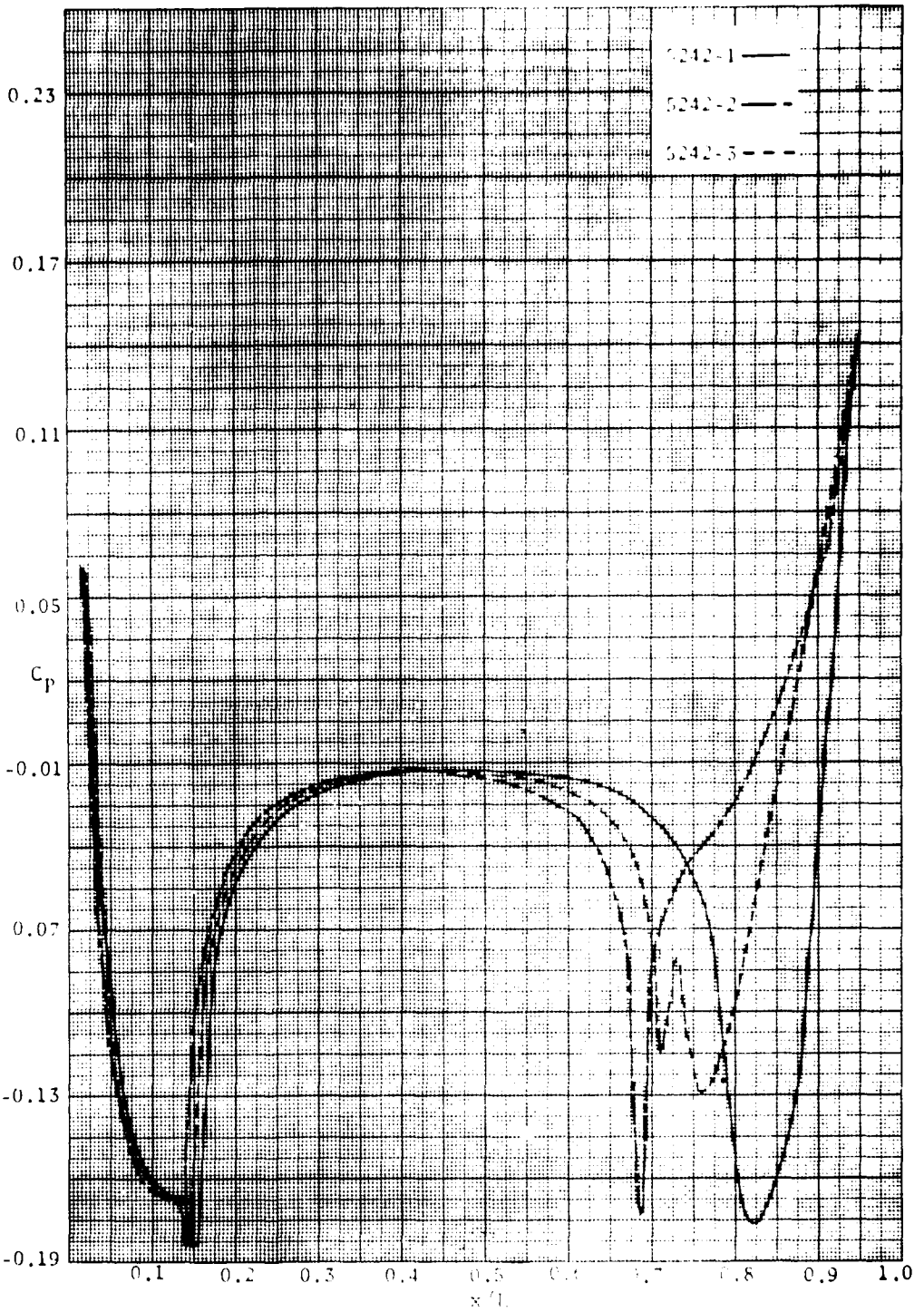

Figure 8A - Series 5242 Pressure Distributions

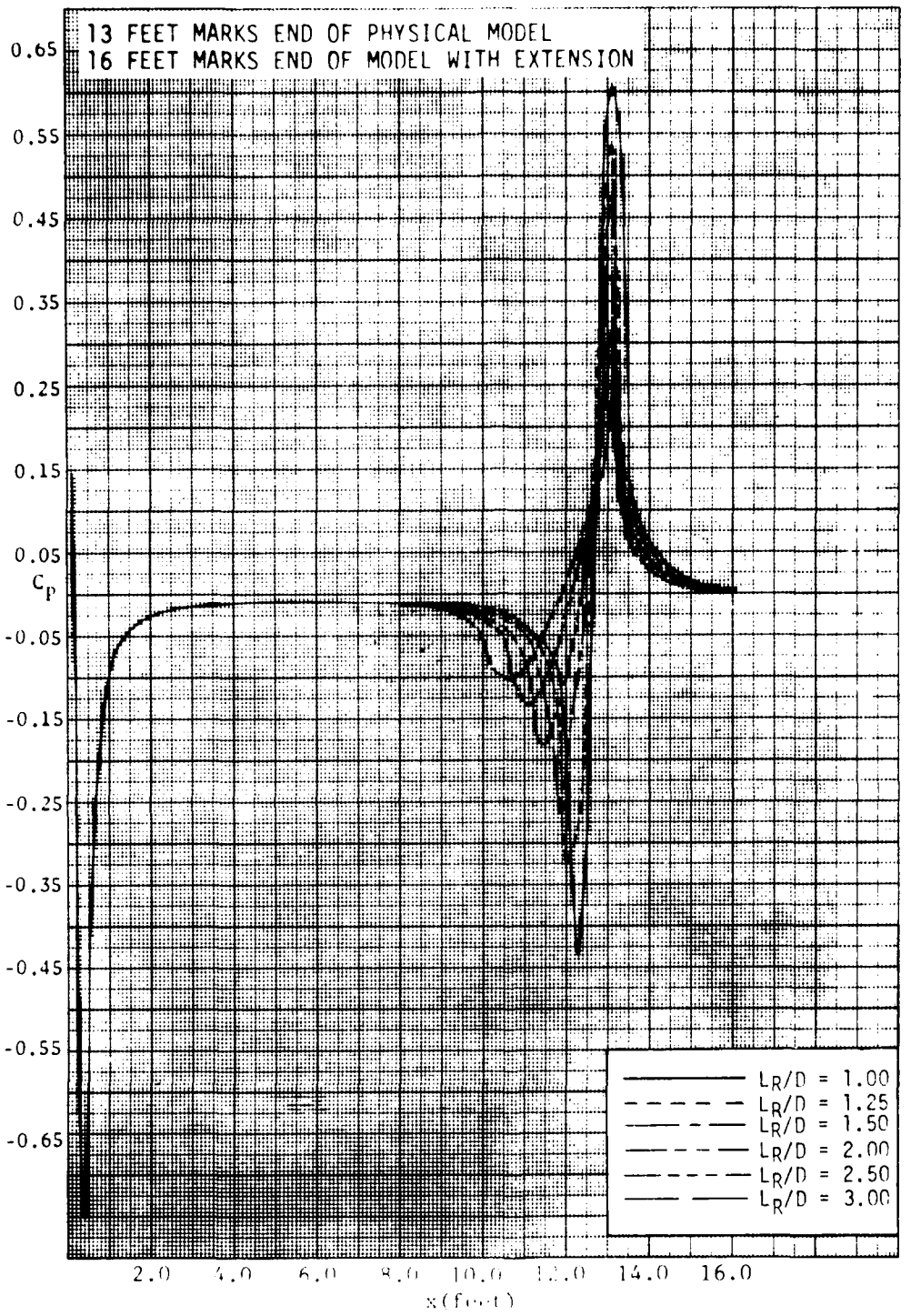

Figure 9A - Kempf Bodies Pressure Distributions

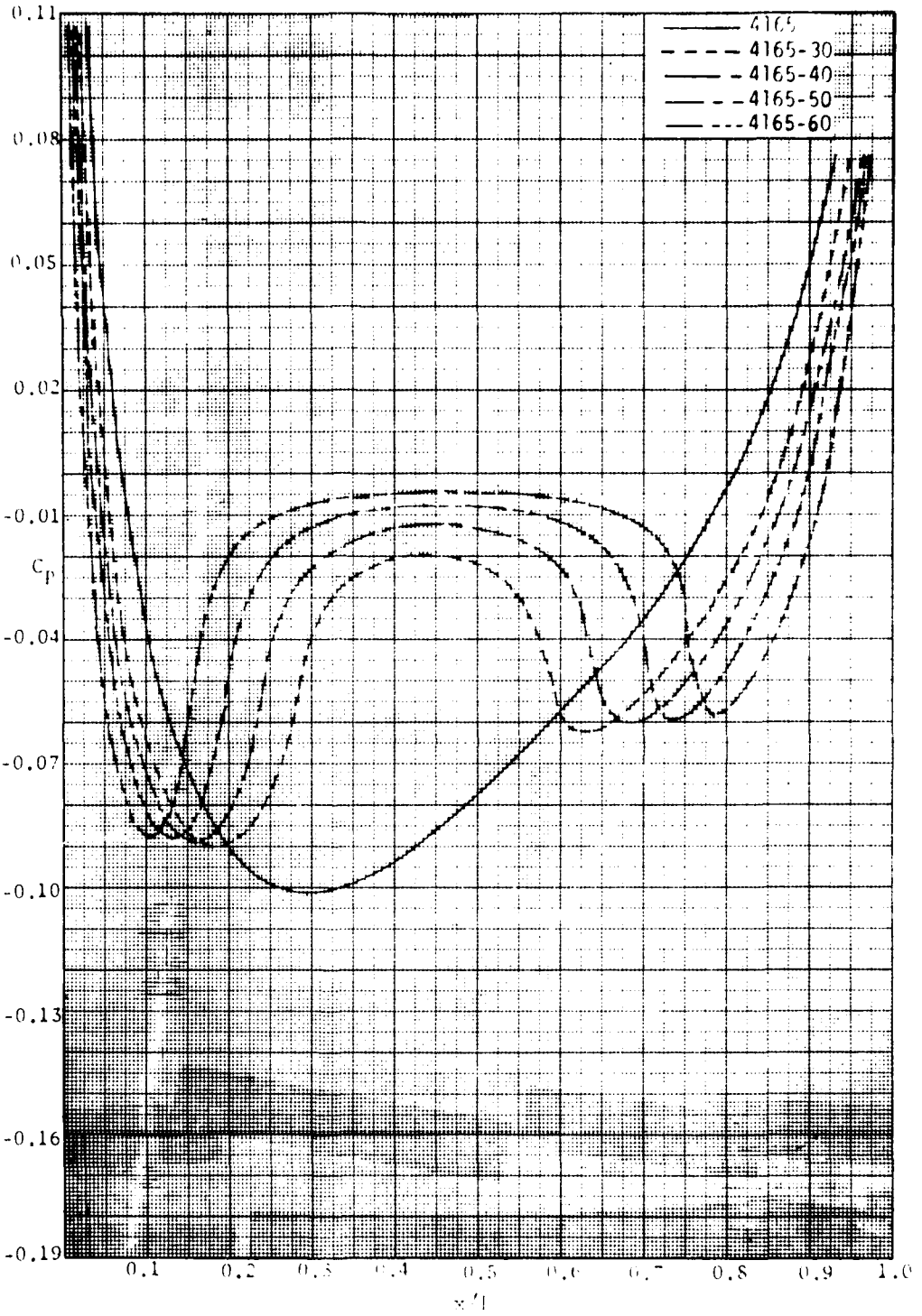

Figure 10A - Series 5x Model 4165 with Parallel Middle Body Pressure Distributions

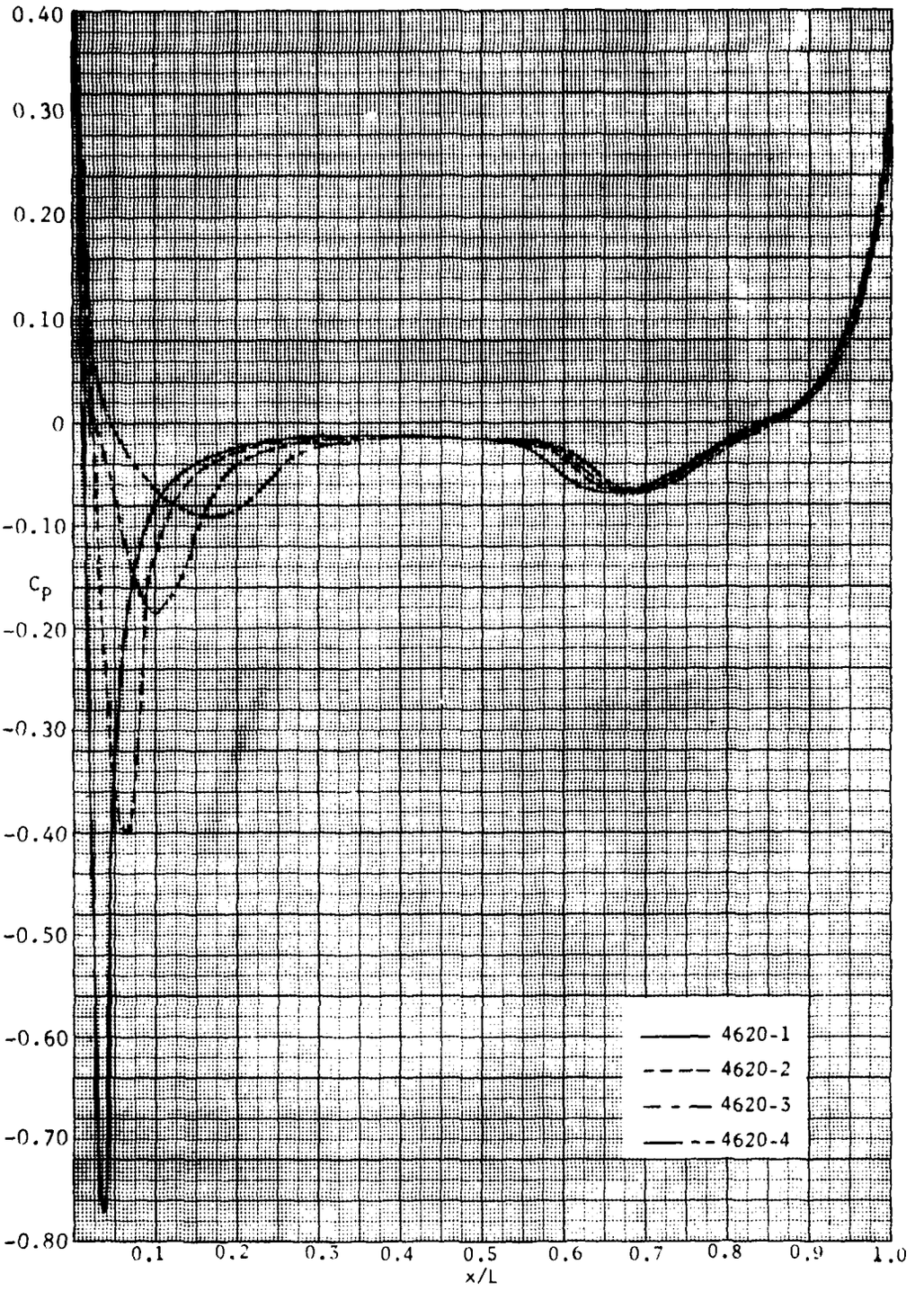

Figure 11A - Series 4620-1, 2, 3, 4 Pressure Distributions

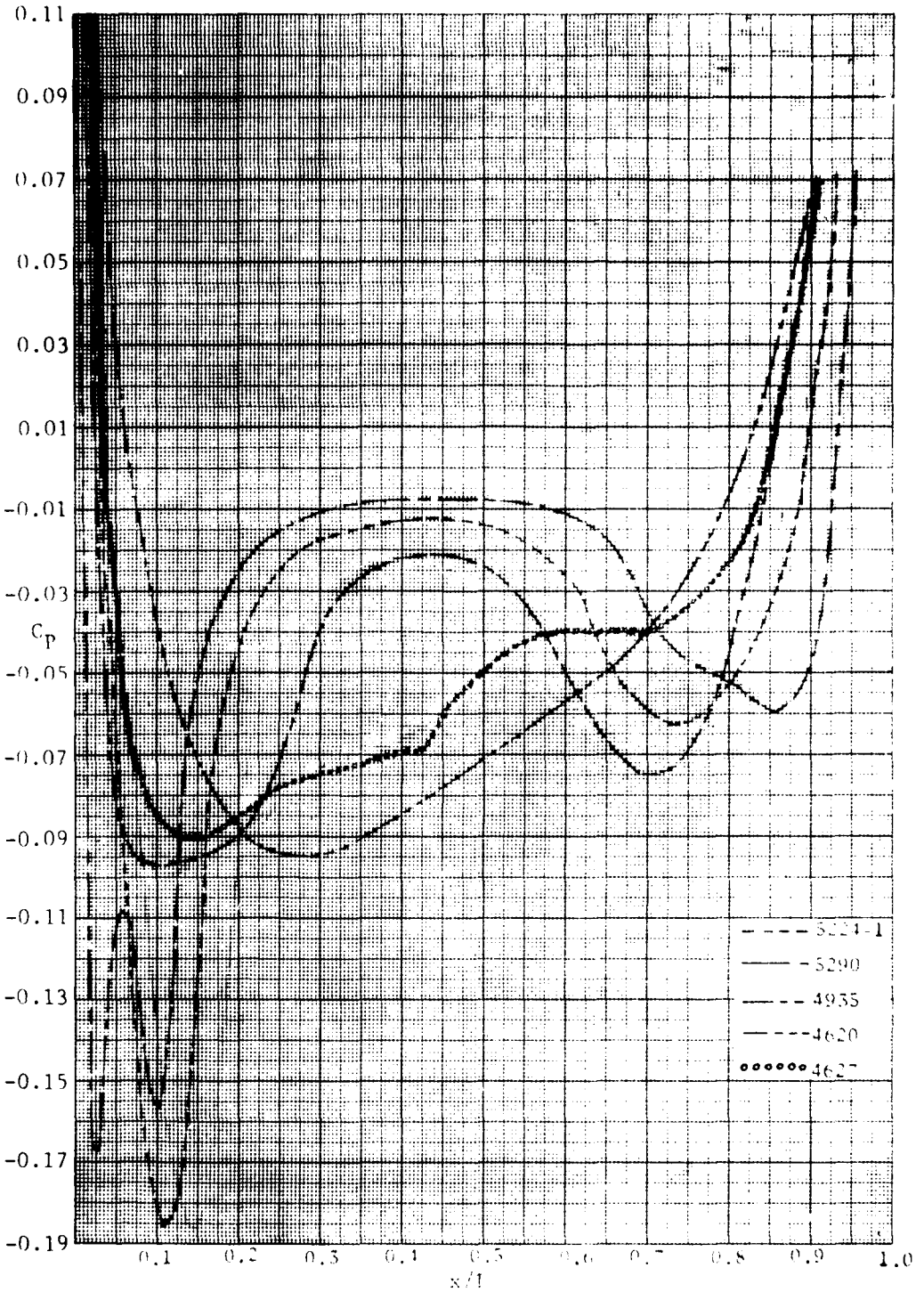

Figure 12A - Pressure Distributions for Miscellaneous Model Forms

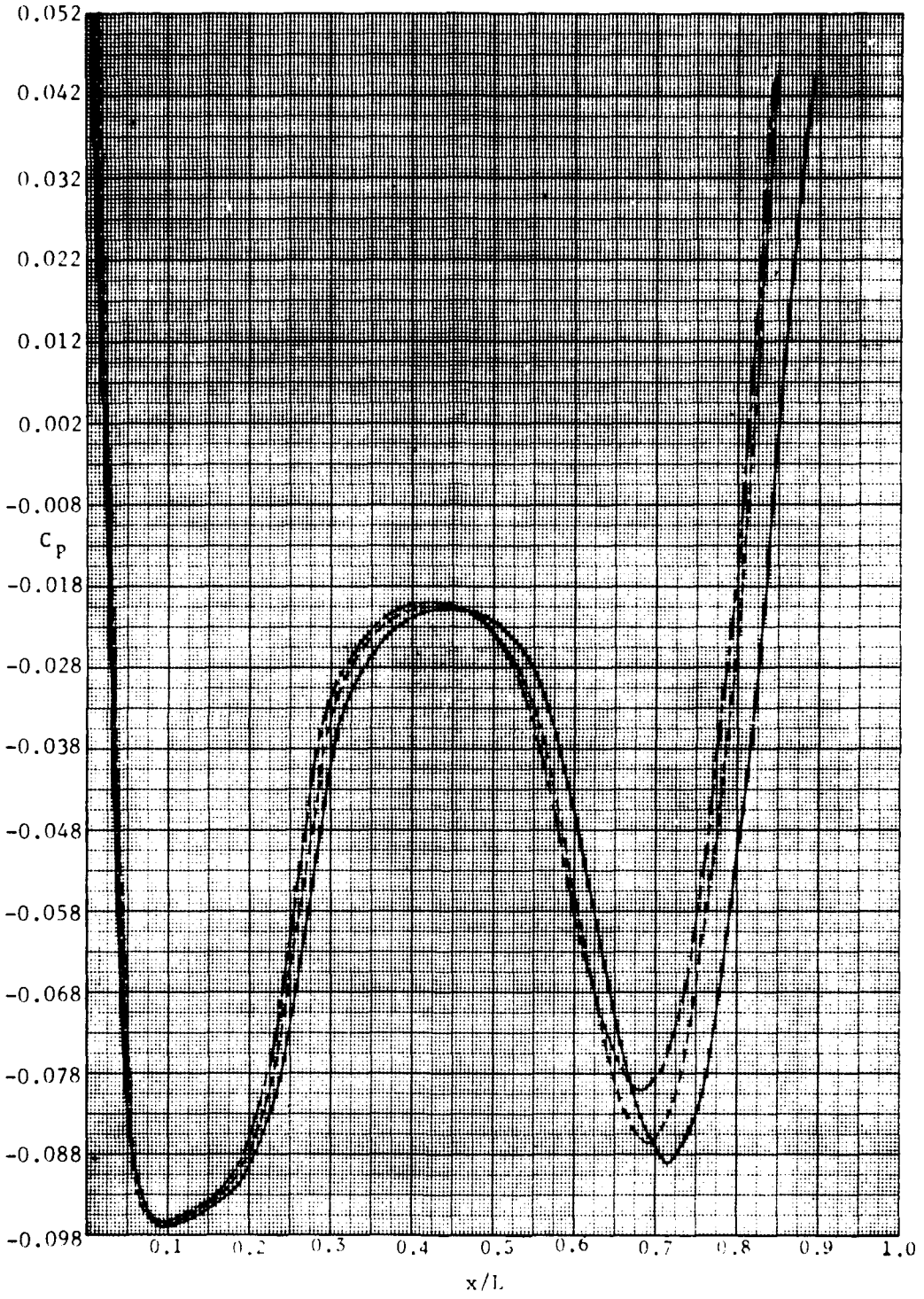

Figure 13A - Pressure Distributions for Series 4935 Extended Tails

REFERENCES

1. Hess, John L. and R.N. James, "On the Problem of Shaping an Axisymmetric Body to Obtain Low Drag at Large Reynolds Numbers," McDonnell Douglas Corporation Report MDC-J6791 (Jan 1975).

2. Hess, John L., "On the Problem of Shaping an Axisymmetric Body to Obtain Low Drag at Large Reynolds Numbers," Journal of Ship Research, Vol. 20, No. 1 (May 1976).

3. Gertler, Morton, "Resistance Experiments on a Systematic Series of Streamlined Bodies of Revolution - For Application to the Design of High-Speed Submarines," David Taylor Model Basin Report C-297 (Apr 1950), declassified 27 Jan 1967.

4. Young, A.D., "The Calculation of the Total and Skin Friction Drag of Bodies of Revolution at Zero Incidence," Aeronautical Research Committee R&M Report 1874 (Apr 1939).

5. Granville, P.S., "The Calculation of the Viscous Drag of Bodies of Revolution," David Taylor Model Basin Report 849 (Jul 1953).

6. Schlicting, H., Boundary Layer Theory, McGraw Hill, New York (1968).

7. Granville, P.S., "Partial Form Factors from Equivalent Bodies of Revolution for the Froude Method of Predicting Ship Resistance," SNAME First Ship Technology and Research Symposium, Washington, DC (Aug 1975).

8. Truckenbrodt, E., "A Method of Quadrature for Calculation of the Laminar and Turbulent Boundary Layer in Case of Plane and Rotationally Symmetrical Flow," NACA TM Report 1379 (May 1955).

9. Falkner, V.N., Aircraft Engineering, 15 (1943), p. 65.

10. Hess, J.L. and A.M.O. Smith, "Calculation of Potential Flow About Arbitrary Bodies," in "Progress in Aeronautical Sciences," Pergamon Press, Oxford and New York, Vol. 8 (1966), pp. 1-138.

11. Kempf, George, "Resistance and Wake of Some Bodies of Revolution," from "New Developments in Ship Research," Jahrbuch Schiffbautechnischen Gesellschaft (1927), pp. 177-178.

12. Kempf, George, "Turbulent Separation on Full Ship Forms," Schiff und Hafen, Vol. 6, No. 7, Hamburg (1954).

13. Larsen, C.A., "Additional Tests of Series 58 Forms, Part 1, Resistance Tests of a Parallel Middle Body Series," David Taylor Model Basin Report C-738 (Nov 1955), declassified on 2 Sep 1975.

14. McCarthy, J.H., J. Power, and T.T. Huang, "The Roles of Transition, Laminar Separation and Turbulence Stimulation in the Analysis of Axisymmetric Body Drag," to be published in the Proceedings of the Eleventh ONR Symposium on Naval Hydrodynamics, sponsored by the Office of Naval Research, London (Mar 1976).

15. Landweber, L. and Matilde Macagno, "Potential Flow about Series 58 Bodies in General Translational and Rotational Motion," Naval Ship Research and Development Center Report 2505 (Jun 1967).

16. Schoenherr, K.E., "Resistance of Flat Surfaces Moving Through a Fluid," Transactions, Society of Naval Architects and Marine Engineers, Vol. 40 (1932).

17. Granville, P.S., "Geometrical Characteristics of Noses and Tails for Parallel Middle Bodies," Naval Ship Research and Development Center Report 3763 (Dec 1972).

18. Granville, P.S., "Geometrical Characteristics of Streamlined Shapes," Naval Ship Research and Development Center Report 2962 (Mar 1969).

INITIAL DISTRIBUTION

Copies	
1	CHONR
	1 Code 438
1	NRL
2	USNA
	1 Lib
	1 Bruce Johnson
1	NAVPGSCOL
1	NROTC & NAVADMINU, MIT
3	NAVUSEACEN, San Diego
	1 M. Reishman
	1 T. Lang
	1 J.W. Hoyt
1	NSWC, White Oak
1	NUSC NPT
7	NAVSEASYSCOM
	1 SEA 03
	1 SEA 0351
	2 PMS 393
	2 PMS 395
	1 PMS 396
2	Mass Inst of Technol
	Dept of Ocean Eng
	1 Lib
	1 P. Mandel
1	Univ of Maryland
	Dept of Mech Eng
	1 Dr. Colin Marks
1	Univ of Michigan
	Dept of NAME
2	Penn State Univ
	Ordnance Research Lab
	1 R.E. Henderson
	1 B.R. Parkin

Copies	
7	NAVSEC
	1 SEC 6113C
	1 SEC 6110.01
	1 SEC 6114
	2 SEC 6114C
	2 SEC 6136
12	DDC
1	NASA HQS
1	National Science Foundation
	Eng Sci Div
1	Univ of Bridgeport
	E.M. Uram, Dept Mech Eng
1	Univ of Calif, Berkeley
	Dept of NA
2	Calif Inst of Technol
	1 A.J. Acosta
	1 D. Coles
1	Catholic Univ
	Dept of Mech Eng
2	Iowa State Univ
	Inst of Hydraulic Res
	1 L. Landweber
1	Adv Tech Center
	C.S. Wells, Jr.
1	Oceanics, Inc.
	A. Lehman
1	Rand Corp
1	Westinghouse Electric
	M.S. Macovsky
1	Univ of Rhode Island
	1 F.M. White,
	Dept Mech Eng

Copies

1 VPI

1 SNAME

1 Boeing Aircraft,
Seattle, Wash.

2 Douglas Aircraft,
Long Beach, Calif
1 T. Cebeci
1 J. Hess

1 Exxon Math & Systems, Inc.
R. Bernicker

1 Hydronautics, Inc.

CENTER DISTRIBUTION

Copies	Code	
1	1500	
1	1504	
1	1520	
1	1524	
1	1540	
1	1541	
3	1552	J. McCarthy
15	1552	N. White
1	1556	
1	1560	
1	184	
1	1843	
1	1900	
1	1942	
30	5214.1	Reports Distribution
1	522.1	Library (C)
1	522.2	Library (A)